DELHI TECHNOLOGICAL UNIVERSITY

(Formerly Delhi College of Engineering)
Shahbad Daulatpur, Main Bawana Road, Delhi-110042, India

PLAGIARISM VERIFICATION

Title of the Thesis: Design and Simulation of a Pocket-Engineered Dielectric-Modulated TFET Biosensor for Label-Free Breast Cancer Detection

Total Pages: 51 **Name of the Scholar:** Shishir Bhargav

Supervisor: Dr. Sumit Kale

Department: Electronics and Communication Engineering

This is to report that the above thesis was scanned for similarity detection. Process and outcome is given below:

Software used: Turnitin **Similarity Index:** 9%

Total Word Count: 13,078 **Date:** May 26, 2026

Candidate's Signature **Signature of Supervisor**

Shishir Thesis Plag Shishir Thesis Plag

Shishir thesis plag

Quick Submit

Quick Submit

Delhi Technological University

Document Details

Submission ID

trn:oid:::1:3579214947

Submission Date

May 26, 2026, 9:47 AM GMT+5:30

Download Date

May 26, 2026, 9:50 AM GMT+5:30

File Name

Shishir_Bhargav_thesis.pdf

File Size

3.4 MB

51 Pages

13,078 Words

67,126 Characters

*% detected as AI

AI detection includes the possibility of false positives. Although some text in this submission is likely AI generated, scores below the 20% threshold are not surfaced because they have a higher likelihood of false positives.

Caution: Review required.

It is essential to understand the limitations of AI detection before making decisions about a student's work. We encourage you to learn more about Turnitin's AI detection capabilities before using the tool.

Disclaimer
Our AI writing assessment is designed to help educators identify text that might be prepared by a generative AI tool. Our AI writing assessment may not always be accurate (i.e., our AI models may produce either false positive results or false negative results), so it should not be used as the sole basis for adverse actions against a student. It takes further scrutiny and human judgment in conjunction with an organization's application of its specific academic policies to determine whether any academic misconduct has occurred.

DESIGN AND SIMULATION OF A POCKET-ENGINEERED DIELECTRIC-MODULATED TFET BIOSENSOR FOR LABEL-FREE BREAST CANCER DETECTION

Thesis Submitted in Partial Fulfillment of the Requirements for the Degree of

MASTER OF TECHNOLOGY

in

VLSI Design and Embedded Systems

by

Shishir Bhargav
(Roll No. 2K24/VLS/10)

Under the Supervision of

Dr. Sumit Kale
(Assistant Professor)

Department of Electronics and Communication Engineering

DELHI TECHNOLOGICAL UNIVERSITY
(Formerly Delhi College of Engineering)
Shahbad Daulatpur, Main Bawana Road, Delhi-110042, India

May, 2026

DELHI TECHNOLOGICAL UNIVERSITY

(Formerly Delhi College of Engineering)

Shahbad Daulatpur, Main Bawana Road, Delhi-110042, India

CANDIDATE'S DECLARATION

I, **Shishir Bhargav**, hereby certify that the work which is being presented in the thesis entitled **"Design and Simulation of a Pocket-Engineered Dielectric-Modulated TFET Biosensor for Label-Free Breast Cancer Detection"** in partial fulfillment of the requirements for the award of the Degree of Master of Technology, submitted in the Department of Electronics and Communication Engineering, Delhi Technological University is an authentic record of my own work carried out during the period from July 2025 to May 2026 under the supervision of **Dr. Sumit Kale**.
The matter presented in the thesis has not been submitted by me for the award of any other degree of this or any other Institute.

Candidate's Signature

DELHI TECHNOLOGICAL UNIVERSITY
(Formerly Delhi College of Engineering)
Shahbad Daulatpur, Main Bawana Road, Delhi-110042, India

CERTIFICATE BY THE SUPERVISOR

Certified that **Shishir Bhargav (Roll No. 2K24/VLS/10)** has carried out the research work presented in this thesis entitled **"Design and Simulation of a Pocket-Engineered Dielectric-Modulated TFET Biosensor for Label-Free Breast Cancer Detection"** for the award of Master of Technology from the Department of Electronics and Communication Engineering, Delhi Technological University, Delhi, under my supervision. The thesis embodies results of original work, and studies are carried out by the student himself and the contents of the thesis do not form the basis for the award of any other degree to the candidate or to anybody else from this or any other University/Institution.

Signature
Dr. Sumit Kale
Supervisor & Assistant Professor
Dept. of Electronics & Communication Eng.
Delhi Technological University

Date:

DELHI TECHNOLOGICAL UNIVERSITY
(Formerly Delhi College of Engineering)
Shahbad Daulatpur, Main Bawana Road, Delhi-110042, India

PLAGIARISM VERIFICATION

Title of the Thesis: Design and Simulation of a Pocket-Engineered Dielectric-Modulated TFET Biosensor for Label-Free Breast Cancer Detection

Total Pages: ______________ **Name of the Scholar:** Shishir Bhargav

Supervisor: Dr. Sumit Kale

Department: Electronics and Communication Engineering

This is to report that the above thesis was scanned for similarity detection. Process and outcome is given below:

Software used: Turnitin **Similarity Index:** __________

Total Word Count: ______________ **Date:** ______________

Candidate's Signature **Signature of Supervisor**

DESIGN AND SIMULATION OF A POCKET-ENGINEERED DIELECTRIC-MODULATED TFET BIOSENSOR FOR LABEL-FREE BREAST CANCER DETECTION

ABSTRACT

This research involves a complete simulation evaluation of a dielectric-modulated Tunnel Field-Effect Transistor (DM-TFET) biosensor intended for the label-free detection of breast cancer cell lines. Possible fabrication steps for the proposed device are also presented. The device displays large differences in its electrical properties by using the various dielectric properties of healthy cells (MCF-10A) and numerous cancer cells, notably Hs578T, MDA-MB-231, MCF7, and T47D. I_{ON} increases with the increase in the dielectric constant of immobilized cell, as found from simulation studies. The device shows a maximum Threshold Voltage Sensitivity (ΔV_{th}) of 130 mV and Transconductance Sensitivity (S_{gm}) of 228 for T47D cells over an air-filled cavity. It is obtained a selectivity factor of 29.6 and a peak Drain Current Sensitivity (S_{Ids}) of 606 with respect to healthy cells. The obtained sharp subthreshold swing (SS) of 94.3 mV/dec shows that the proposed sensor has a great potential for fast and highly accurate biological diagnostics.

ACKNOWLEDGEMENTS

I am very thankful to my supervisor Dr. Sumit Kale for his valuable guidance, constant motivation and critical comments on this research work. His expertise in biosensors and in modeling semiconductor devices has been crucial to the shaping of this thesis.

I am very thankful to the faculty members, lab staff and research Ph.D. scholars of Department of Electronics and Communication Engineering of Delhi Technological University for providing the facilities, technical guidance and software tools needed for running the TCAD simulations. Finally, I would like to thank my parents and colleagues for their constant support and understanding during the preparation of this dissertation report.

Shishir Bhargav

TABLE OF CONTENTS

Certificate **i**

Abstract **iv**

Acknowledgements **v**

List of Tables **viii**

List of Figures **ix**

List of Symbols and Abbreviations **x**

1 CHAPTER 1: INTRODUCTION **1**
1.1 Clinical Background of Breast Cancer and diagnostic challenges . . . 1
1.2 Point-of-Care Diagnostics and Label-Free Biosensing Concepts 2
1.3 Dielectric Modulation Picture and Solid State Interfaces 2
1.4 The Subthreshold Swing Constraint and the Boltzmann Tyranny . . 3
1.5 Steep Slope Core Sensors using Tunnel Field Effect Transistors 3
1.6 Structural innovations in pocket engineering and heterojunction . . . 4
1.7 Structure of the Thesis Document 5

2 CHAPTER 2: REVIEW OF LITERATURE AND PROBLEM IDENTIFICATION **6**
2.1 Subthreshold and the thermionic limit Bottleneck Swing 6
2.2 Physics of dielectric modulation for label-free detection 7
2.3 Steep Slope Core Sensors: Tunnel Field-Effect Transistors 7
2.4 Literature Trends: Engineering Critical Analysis 8
2.5 Identification of the Central Research Gap 8
2.6 Scope and Objectives of the Present Dissertation 9

3 CHAPTER 3: DEVICE ARCHITECTURE AND TCAD SIMULATION METHODOLOGY **11**
3.1 Device Architecture 11
3.2 Simulation Models 12
3.3 Fabrication Process Flow 13

4 CHAPTER 4: RESULTS AND DISCUSSION **15**
4.1 DC Characteristics 15
4.2 Surface Potential and Electric Field Analysis 17
4.3 Static & Dynamic Parameter Analysis 18
4.4 Selectivity Analysis 19
4.5 Sensitivity Analysis 20
4.5.1 Threshold Voltage Sensitivity (ΔV_{th}) 20

4.5.2 Sensitivities of Drain Currents (SIDs) 20
4.6 Impact of Biomolecule Occupancy 23
4.7 Performance Evaluation 24

5 CHAPTER 5: CONCLUSION, FUTURE SCOPE AND SOCIAL IMPACT 25
5.1 Summary of Key Research Findings 25
5.2 Future Scope and Social Impact 25

REFERENCES 26

LIST OF PUBLICATIONS 29

APPENDIX A: SILVACO ATLAS SIMULATION SCRIPT 30

LIST OF TABLES

3.1 Design Parameters of the Proposed TFET Biosensor 12

4.1 Various Cell Lines with Corresponding Dielectric Constants (k) . . . 15
4.2 Benchmark Comparison: TFET Biosensor Sensitivity 24

LIST OF FIGURES

3.1 Cross-sectional schematic of the proposed pocket-engineered TFET biosensor with annotated device dimensions conforming to Table 3.1. 11
3.2 Proposed fabrication process flow for the TFET biosensor: (a) SOI Substrate Preparation; (b) Ion Implantation for Source/Drain; (c) Epitaxial Growth of InAs Pocket; (d) Channel Etching to define dual-thickness; (e) High-κ Dielectric Deposition; (f) Oxide Patterning; (g) Sacrificial material and Low-κ Deposition; (h) Sacrificial Etch for Nanocavity and Metal Gate Deposition; (i) Backside Etching; (j) Finalization, wafer bonding, and Contact Metallization. . 14

4.1 Drain current versus gate voltage linear plot I_{ds} vs. V_{gs}. 16
4.2 Logarithmic plot of Drain Current (I_{ds}) versus Gate Voltage (V_{gs}). . . 16
4.3 Surface potential variation along the channel length for different cell lines. 17
4.4 Distribution of electric field across the channel length. 17
4.5 Threshold voltage (V_{th}) and on-state current (I_{ON}) variation with cell type. 18
4.6 Gm (transconductance) vs. V_{gs} (gate voltage) for all the cell lines. . . 18
4.7 Peak Transconductance (g_m) and Subthreshold Swing (SS) obtained for each cell type. 19
4.8 Selectivity of the biosensor normalized to the healthy MCF-10A cell. 20
4.9 Fig. 4.9. Sensitivity of the Threshold Voltage (ΔV_{th}) with respect to Air. 21
4.10 Drain Current Sensitivity (S_{Ids}) versus Gate Voltage. 21
4.11 ON-Current Sensitivity (S_{Ion}) at $V_{gs} = 2.0$ V. 22
4.12 Transconductance Sensitivity (S_{gm}) relative to Air. 22
4.13 Impact of occupancy on transfer characteristics for healthy MCF-10A cells. 23
4.14 Impact of occupancy on transfer characteristics for high-risk T47D cells. 23
4.15 Vth and I_{ION} versus occupancy for MCF-10A vs. T47D. 24

LIST OF SYMBOLS, ABBREVIATIONS AND NOMENCLATURE

TFET	—	Tunnel Field-Effect Transistor
MOSFET	—	Metal-Oxide-Semiconductor Field-Effect Transistor
DM-TFET	—	Dielectric-Modulated Tunnel Field-Effect Transistor
BTBT	—	Band-to-Band Tunneling
TCAD	—	Technology Computer-Aided Design
CMOS	—	Complementary Metal-Oxide-Semiconductor
POC	—	Point-of-Care
ELISA	—	Enzyme-Linked Immunosorbent Assay
SS	—	Subthreshold Swing
SRH	—	Shockley-Read-Hall
CVT	—	Lombardi Mobility Model Component
k	—	Dielectric Constant
$\mathbf{V_{th}}$	—	Threshold Voltage
$\mathbf{I_{ON}}$	—	On-State Current
$\mathbf{g_m}$	—	Transconductance

Chapter 1

INTRODUCTION

1.1 Clinical Background of Breast Cancer and diagnostic challenges

Malignant oncology is still one of the biggest public health problems of the modern era and breast cancer is the leading cause of mortality and incidence of cancer in women worldwide [1]. Demographic assessments and epidemiological reviews indicate a growing trend of diagnosis in all regions of the world, developed and developing, making early detection a critical clinical necessity [2, 3].

Survival rates are heavily dependent on the clinical stage at diagnosis. If the malignant transformation is detected early, while it is still localized to the primary epithelial tissues, the five-year survival rate is over 90%. However, in cases of regional or distant metastasis, treatment options are limited and the survival rates are significantly reduced.

Major operational bottlenecks plague conventional diagnostic pathways despite the critical need for early detection. The standard screening methods are mammography, magnetic resonance imaging (MRI), propagation-based phase-contrast tomography and high-resolution ultrasound networks [6]. These systems provide structural information, but they often have difficulties in detecting micro-calcifications or subtle tumor shapes in the early development stages leading to false-negative results.

Clinical workflows confirm suspicious screening results by tissue biopsies followed by histopathological verification, or serum-based protein biomarker tracking using Enzyme-Linked Immunosorbent Assays (ELISA) [5]. These sophisticated laboratory workflows are highly accurate but depend on complex infrastructure, expensive chemical reagents and significant processing time. Such a delay in reporting may slow down clinical decision making and adversely affect the patient's prognosis.

1.2 Point-of-Care Diagnostics and Label-Free Biosensing Concepts

Clinical research is shifting to decentralized Point-of-Care (POC) diagnostic paradigms to overcome the constraints of centralized laboratory testing. A practical POC system should be small, inexpensive, easy to use without special training, and able to provide fast and reliable readouts directly in resource-limited settings [4]. To achieve these goals, the shift from traditional label-based bio-detection methods to direct label-free electronic detection frameworks is required.

The most common labeled sensing strategies are based on the conjugation of a secondary reporter agent (fluorescent dye, radioactive isotope or active enzyme) to the target analyte to generate a measurable output signal. This labelling is sensitive but complicated by multiple washing steps, precise chemical preparation and expensive optical reading systems.

In contrast, label-free solid-state biosensing networks directly sense biological binding events. Binding of a target molecule or whole cell to the sensor surface leads to an immediate change in the local electrical properties, e.g. interface potential, capacitive coupling or current density. This simple conversion of biological interactions into electronic signals eliminates the need for complex chemical processing, reduces the cost of testing and enables real-time diagnostic platforms that are compatible with mass production.

1.3 Dielectric Modulation Picture and Solid State Interfaces

The coupling of solid-state microelectronic devices with biological media has resulted in the development of field-effect transistor (FET) biosensors. Historically, this architecture has been achieved by modifications of conventional Metal-Oxide-Semiconductor Field-Effect Transistor (MOSFET) topologies [5]. This technique eliminates the conventional metal gate electrode and thus directly exposes the underlying gate dielectric insulation layer to the target environment. The surface-immobilized capture receptors interact with target biomolecules having a net electric charge and alter the distribution of their charges and thus modulating the output drain current by changing the electrostatic potential at the channel interface.

However, charge-based field-effect sensing is severely constrained by physical limitations in high salinity physiological buffers due to ionic screening. Mobile counter-ions present in the solution screen the molecular charge of the target analyte and form an electrical double layer that could obscure the binding signal if it occurs outside the characteristic Debye length.

The dielectric modulation framework has been proposed to overcome this limitation. A physical nanocavity is etched directly in the gate oxide stack, taking advantage of the intrinsic dielectric properties of the biological target, instead of the net charge of a molecule. The introduction of a target biological specimen

into the sensing nanogap replaces the empty air medium ($k = 1.0$), changing the overall gate capacitance and modulating the device electrical characteristics.

1.4 The Subthreshold Swing Constraint and the Boltzmann Tyranny

While dielectric-modulated MOSFET biosensors offer a viable approach for label-free screening, their practical performance is fundamentally limited by a core physical barrier known as the Boltzmann tyranny [9]. In any standard field-effect transistor operating via thermionic carrier injection, electrons must overcome an energy barrier at the source-channel junction through thermal activation. The efficiency of this switching behavior is measured by the subthreshold swing (SS), which reflects the change in gate voltage required to alter the output current by one order of magnitude:

$$SS = \frac{dV_{gs}}{d(\log_{10} I_{ds})} = \ln(10) \cdot \frac{k_B T}{q} \cdot \left(1 + \frac{C_d}{C_{ox}}\right) \tag{1.1}$$

where k_B is the Boltzmann constant, T is the absolute operating temperature, q is the elementary electronic charge, C_d is the depletion layer capacitance, and C_{ox} is the gate oxide capacitance stack. At room temperature ($T = 300$ K), this physical mechanism sets an absolute theoretical lower floor:

$$SS_{\text{limit}} = \ln(10) \cdot \frac{k_B T}{q} \approx 59.6 \text{ mV/decade} \tag{1.2}$$

As C_{ox} drops, the body factor factor ($(1 + C_d/C_{ox})$) increases significantly, often surpassing the practical subthreshold swing of MOSFET biosensors beyond 120 mV/decade [11, 10]. Subthreshold degradation reduces the voltage sensitivity margin of the device, increases the static power leakage (I_{OFF}) and can mask subtle biological signals behind the thermal noise floors, rendering the standard MOSFET configurations impractical for ultra-low power portable screening nodes.

1.5 Steep Slope Core Sensors using Tunnel Field Effect Transistors

Tunnel Field Effect Transistors (TFETs) have been proposed as a promising steep-slope alternative for high-sensitivity solid-state biosensing to overcome the limitations of thermionic injection barrier [12]. A TFET utilizes the quantum mechanical Band-to-Band Tunneling (BTBT) through an asymmetric heavily doped $p^+ - i - n^+$ junction structure [9] which completely alters the carrier injection mechanism.

When the device is off, the huge energy barrier between the valence band edge of the p^+ source and the conduction band edge of the intrinsic channel prevents

carrier transport, resulting in ultra-low leakage. A positive gate bias pulls down the energy bands inside the channel region sharply, leading to a narrow spatial tunneling window at the junction interface. We model the carrier generation rate in this localized tunneling barrier using Kane's expression:

$$G_{\mathrm{BTBT}} = A_{\mathrm{Kane}} \cdot \frac{E^2}{E_g^{1/2}} \cdot \exp\left(-B_{\mathrm{Kane}} \cdot \frac{E_g^{3/2}}{E}\right) \tag{1.3}$$

where E is the localized electric field profile across the junction, E_g is the material energy bandgap, and $A_{\mathrm{Kane}}, B_{\mathrm{Kane}}$ are material-dependent scaling constants [25].

Since the carrier generation rate depends exponentially on the local electric field (E), changes in the gate capacitance due to dielectric cavity modulation scale the output drive current (I_{ds}) exponentially [14]. This steep current response enables TFET architectures to overcome the Boltzmann limit and achieves subthreshold swing values well below the thermionic floor ($SS < 60$ mV/dec) at room temperature, providing exceptional sensitivity to subtle changes in cavity permittivity [13, 7].

1.6 Structural innovations in pocket engineering and heterojunction

Silicon-based homojunction TFET devices exhibit excellent subthreshold swing properties. They however often suffer from low on-state drive currents (I_{ON}) due to the relatively large effective mass of electrons in bulk silicon and its wide indirect bandgap. To overcome this drive current bottleneck, and to maximize the sensitivity margins, two major structural innovations are incorporated in modern TFET architectures: pocket engineering and heterojunction material design [19, 22].

Pocket engineering: introduction of an ultra-thin, highly doped semiconductor region at the source-channel interface. This localized dopant density significantly enhances the electric field gradient in the junction, reducing the depletion width and greatly enhancing the tunnelling probability. This pocket can be implemented with other low bandgap materials such as Indium Arsenide (InAs) to have heterojunction interface for further improvement of transport kinetics.

The small bandgap of InAs lowers the height of the potential barrier for carriers to cross, greatly enhancing the rate of band-to-band tunneling. This pocket-engineered heterojunction configuration, along with a dielectrically modulated gate nanocavity, ensures that small variations in target cell permittivity result in large and readily detectable variations in output current, providing an excellent framework for high-sensitivity whole-cell screening platforms [8].

1.7 Structure of the Thesis Document

The research and engineering characterization work presented in this dissertation report is organized systematically into five main chapters:

- **Chapter 1: Introduction** gives a brief overview of early clinical paradigms of breast cancer diagnostics, the requirements of point-of-care testing, the basics of label-free solid-state sensing, limitations of field-effect device physics and the key structural objectives of this project.
- **Chapter 2: Literature Review and Problem Identification:** A survey on previous engineering trends, various device topologies, charge plasma modeling rules, a detailed analysis of recent literature benchmarks, and a formal statement of the research gaps and project objectives.
- **Chapter 3: Device Architecture and TCAD Simulation Methodology** discusses the exact architectural coordinate layout, material compositions, asymmetric high-k/low-k gate stack optimizations, and physical simulation models calibrated in the Silvaco ATLAS TCAD environment along with a feasible CMOS-compatible process integration flow.
- **Chapter 4: Results and Discussion** contains the full set of numeric observation data including linear and logarithmic transfer responses, surface electrostatic potential profiles, junction electric field distributions, transconductance curves, selectivity ratios, voltage sensitivity metrics, and a full analysis of partial cavity occupancy variations.
- **Chapter 5: Conclusion, Future Scope and Social Impact** summarizes the main research outcomes, evaluates the immediate clinical and social impact of decentralized screening platforms and discusses future technological research directions for multi-target microfluidic on-chip integration.

Chapter 2

REVIEW OF LITERATURE AND PROBLEM IDENTIFICATION

2.1 Subthreshold and the thermionic limit Bottleneck Swing

Solid state field-effect architectures are commonly employed in modern point-of-care diagnostics. Traditionally, conventional MOSFET topologies have been modified for label free biological sensing by directly exposing the gate dielectric layer to biological targets [5]. In these classical designs, the injection of carriers from the source to the channel is controlled by thermionic emission over a controllable potential barrier.

Mathematically, the electrostatic switching performance of any thermionic transistor is bounded by its subthreshold swing (SS):

$$SS = \frac{dV_{gs}}{d(\log_{10} I_{ds})} = \ln(10) \cdot \frac{k_B T}{q} \cdot \left(1 + \frac{C_d}{C_{ox}}\right) \tag{2.1}$$

where k_B is the Boltzmann constant, T is the operating temperature, q is the electronic charge, C_d is the depletion layer capacitance and C_{ox} is the gate oxide capacitance. This transport mechanism imposes an absolute physical lower bound at ambient temperature ($T = 300$ K):

$$SS_{\text{limit}} = \ln(10) \cdot \frac{k_B T}{q} \approx 59.6 \text{ mV/decade} \tag{2.2}$$

called the Boltzmann thermal limit [9]. The insertion of a physical sensor nanocavity in a typical MOSFET gate stack results in a dramatic decrease of the effective gate capacitance due to the serial insertion of an air gap ($k = 1$). This reduction in C_{ox}, according to Eq. 2.1, leads to a significant degradation of the subthreshold swing, often pushing practical MOSFET biosensors to $SS \geq 120$ mV/decade [11], which reduces voltage sensitivity and results in high standby power leakage.

2.2 Physics of dielectric modulation for label-free detection

Dielectric modulation avoids chemical labels by treating the sensing nanogap as an open dielectric waveguide. When target biological cells are trapped inside the cavity space, they displace the baseline air medium ($k = 1.0$) and change the overall capacitance profile of the gate stack.

The effective capacitance of the dual layer sensing gate insulator is given by:

$$C_{\text{eff}} = \frac{C_{\text{ox}} \cdot C_{\text{cav}}}{C_{\text{ox}} + C_{\text{cav}}} = \frac{\epsilon_0 \cdot \epsilon_{\text{ox}} \cdot \epsilon_{\text{bio}}}{\epsilon_{\text{bio}} \cdot T_{\text{ox}} + \epsilon_{\text{ox}} \cdot T_{\text{cav}}} \tag{2.3}$$

where ϵ_0 is the vacuum permittivity, ϵ_{ox} and ϵ_{bio} are the relative permittivities of the oxide and the target biomolecule, respectively, T_{ox} is the remaining oxide thickness and T_{cav} is the physical thickness of the carved cavity space.

High-κ species bind in the cavity, leading to an instantaneous increase of C_{eff} as ϵ_{bio} moves upwards. This capacitive boost down-shifts the threshold voltage and alters the vertical electric field profile inside the underlying semiconductor channel layer without any external change in the net molecular charge. Precise change of current output and transconductance are mapped for the screening of targets.

2.3 Steep Slope Core Sensors: Tunnel Field-Effect Transistors

The thermionic injection limitation is completely overcome by the Tunnel Field-Effect Transistors (TFET) utilizing quantum mechanical Band-to-Band Tunneling (BTBT) through a designed asymmetric junction [10]. A TFET is a gated $p^+ - i - n^+$ diode design with reverse bias. When a positive gate bias (V_{gs}) is applied, the energy bands are pulled down sharply in the intrinsic channel region, allowing electrons to tunnel directly from the source valence band to the channel conduction band.

The quantum rate of generation of carriers across this confined tunneling barrier takes the non-local analytical expressions of Kane:

$$G_{\text{BTBT}} = A_{\text{Kane}} \cdot \frac{E^2}{E_g^{1/2}} \cdot \exp\left(-B_{\text{Kane}} \cdot \frac{E_g^{3/2}}{E}\right) \tag{2.4}$$

where E is the localized electric field profile across the junction, E_g is the target semiconductor material energy bandgap, and $A_{\text{Kane}}, B_{\text{Kane}}$ are material-dependent scaling constants [25]. The generation rate scales exponentially with junction electric field (E).

Modulation of the dielectric cavity induces fluctuations in the gate capacitance resulting in exponential scaling of the output drive current (I_{ds}). This steep current response enables TFETs to achieve subthreshold swing values well below

the 60 mV/dec thermionic limit ($SS < 60$ mV/dec) at room temperature, causing them to be very sensitive to small electrostatic variations [12].

2.4 Literature Trends: Engineering Critical Analysis

The architectural development from planar silicon devices to complex multi-gate heterojunction architectures has been widely studied in the field of solid-state biosensing. The initial implementation frameworks confirmed that the combination of the TFET devices with a carved dielectric gap allowed variations in cavity permittivity to produce major changes in output tunneling current leading to significantly higher electrical sensitivity margins compared to traditional MOSFET alternatives [14].

For these baseline models there are different design guidelines for different configurations to improve. The investigation of dielectrically modulated dopingless TFET structures has been explored through charge plasma techniques with specified metal work functions to realize virtual source and drain extensions [29]. This approach is effective in mitigating the high thermal budgets and the random dopant fluctuation (RDF) problems of conventional junctions, although the baseline drive currents are limited by the carrier mass in silicon.

Topologies with localized source-side pockets are also investigated to mitigate the drive current bottleneck [30]. One must be careful to consider the constraints due to steric hindrance in the related nanogaps. The introduction of highly doped pocket areas at the tunneling junction reduces the width of the depletion layer, which in turn greatly enhances the carrier injection rates. Simultaneously, the integration of two-dimensional material channels is reported, based on Si-doped MoS_2 thickness-engineered layouts optimized for breast cancer cell screening applications [8]. The study proved that malignant cell lines have higher relative permittivity properties than healthy tissues as a result of variation of intracellular water content and changed protein structures.

More recently, performance enhancement was focused on the incorporation of alternative low bandgap chemicals within pocket-engineered heterojunction frameworks [19, 22]. Adding a thin, epitaxially grown layer of InAs at the source–channel interface forms a pocket and reduces the effective tunneling barrier height, giving much higher overall drive currents. Moreover, it has been reported that the employment of dual symmetric nanocavity arrays can produce robust multi-line whole-cell screening profiles that allow successful classification of different tumor grades from distinct capacitive shifts [20].

2.5 Identification of the Central Research Gap

Despite the above structural and material breakthroughs in the field effect biosensing, a critical appraisal of the current engineering landscape reveals some unresolved challenges:

1. **The On-Current vs. Ambipolarity Tradeoff:** Pocket-engineered homojunction TFETs improve on-state drive currents, but heavy doping in these narrow regions leads to strong ambipolar conduction in negative gate-to-drain bias. This increases static power leakage and decreases the clean sensing window.

2. **Subthreshold Degradation for Low Permittivity Loadings:** The majority of the existing dielectric-modulated TFET biosensors demonstrate a degradation in capacitive coupling when a large portion of the gate stack is transformed into a physical cavity. In tracking lower-permittivity species, the subthreshold swing deteriorates well beyond 100 mV/dec, masking tiny biological signals behind high thermal noise floors.

3. **No Strong Whole-Cell Multi-Line Discriminability with Partial Filling Constraints:** Most models are based on an idealized scenario where biomolecules homogeneously occupy 100% of the nanocavity. In real sample delivery, the filling is usually not complete, the orientation is unpredictable, and there is steric hindrance inside the nanogap. No comprehensive multi-line classification profiles mapping the electrical response of specific breast cancer cell line variants—healthy reference cells (**MCF-10A**, $k = 4.5$) versus malignant lines (**Hs578T**, $k = 22.0$; **MDA-MB-231**, $k = 24.5$; **MCF-7**, $k = 27.5$; and **T47D**, $k = 32.0$)—across varying filling intervals exist.

2.6 Scope and Objectives of the Present Dissertation

This research tackles these limitations by designing, optimizing and evaluating a new Pocket-Engineered Dielectric-Modulated Heterojunction TFET Biosensor tailored for label-free breast cancer cell classification. The explicit objectives of this research work are categorized under three main implementation phases:

- **Junction and Energy-Band Engineering:** Introduce a thin 3 nm InAs pocket layer at the source-channel interface to reduce the effective tunneling barrier height and maximize driving current. This, together with an asymmetric hetero-dielectric gate stack (SiO_2 on the source side for minimizing parasitic capacitance and HfO_2 on the drain side for enhanced electrostatic control) suppresses the ambipolar leakage.

- **Strictly Calibrated TCAD Simulation Platform:** Build and run a complete physics-based numeric simulation matrix using the Silvaco ATLAS environment. This paradigm links non-local quantum band-to-band tunneling dynamics with Lombardi CVT mobility degradation and Shockley-Read-Hall trapping to capture realistic device physics under low-power operating profiles.

- **Whole-Cell Selectivity and Occupancy Robustness Profiling:** Evaluate the electrical response of the device against well-characterized breast cancer cell lines and plot the specified metrics (V_{th}, I_{ds}, g_m, and SS) as a function of permittivity. Finally, monitor performance at discrete cavity filling levels (25%, 50%, 75%, and 100%) to confirm that the sensor generates distinct, noise-immune diagnostic signatures even with partial target loading.

Chapter 3

DEVICE ARCHITECTURE AND TCAD SIMULATION METHODOLOGY

3.1 Device Architecture

The suggested biosensor is based on a TFET architecture integrating a hetero-junction pocket to boost tunneling efficiency. Fig. 3.1 displays the schematic perspective of the proposed TFET biosensor, indicated with crucial geometrical parameters.

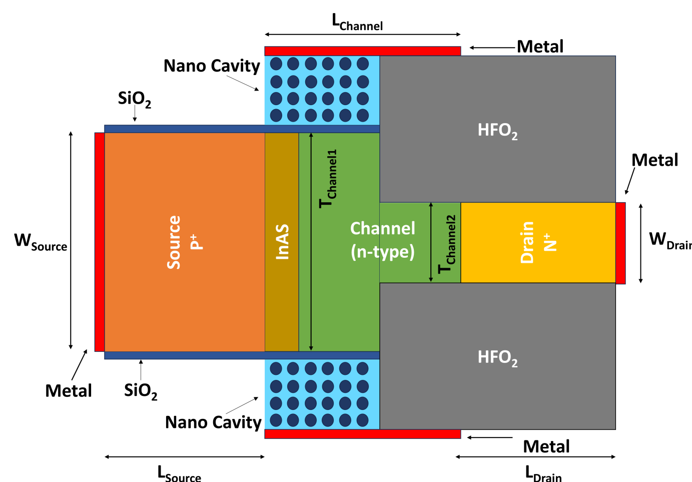

Figure 3.1: Cross-sectional schematic of the proposed pocket-engineered TFET biosensor with annotated device dimensions conforming to Table 3.1.

The particular geometrical dimensions and doping concentrations employed in this simulation are reported in Table 3.1. The device has a channel architecture which provides for aggressive footprint scaling while preserving adequate channel management.

The gate stack features a novel hetero-dielectric configuration to optimize device performance. To improve stability and reduce parasitic capacitance at the

Table 3.1: Design Parameters of the Proposed TFET Biosensor

Parameter	Symbol	Value
Channel Length	L_{channel}	22 nm
Source/Drain Pocket Length	L_{pocket}	3 nm
Nanocavity Length	L_{cav}	11 nm
Nanocavity Width	T_{cav}	5 nm
Gate Oxide Thickness	T_{ox}	1 nm
Thickness of Sensing Cavity	T_{channel1}	15 nm
Control Channel Thickness	T_{channel2}	5 nm
Source Doping (P^+)	N_S	1×10^{20} cm^{-3}
Drain Doping (N^+)	N_D	1×10^{18} cm^{-3}
Channel Doping (N^-)	N_{ch}	1×10^{12} cm^{-3}
Pocket Material	-	InAs
Source Dielectric (Thicker Side)	-	SiO_2
Drain Dielectric (Thinner Side)	-	HfO_2
Gate Work Function	Φ_M	4.1 eV

tunneling junction, a Low-κ dielectric (SiO_2) is used on the source side of the thicker channel (T_{channel1}). On the other hand, the electrostatic control at the drain side, where the channel is narrower (T_{channel2}), is increased by using a High-κ dielectric (HfO_2) [23, 24].

3.2 Simulation Models

The device simulations were performed using the Silvaco ATLAS TCAD tool. To properly forecast the electrical characteristics and biosensing performance, appropriate physical models were calibrated based on known semiconductor physics.

First and foremost, Kane's Band-to-Band Tunneling (BTBT) model is utilized. Since TFETs work by quantum mechanical tunneling rather than thermal emission, standard drift-diffusion models are inadequate. Kane's model calculates the carrier production rate at the source-channel tunneling junction based on the local electric field and the bandgap of the material [25].

To account for trap-assisted recombination, which is crucial for simulating leakage currents in the subthreshold regime (the "off" state), the Shockley-Read-Hall (SRH) recombination model is incorporated [17]. This guarantees realistic and non-artificially low simulated off-currents (I_{OFF}).

Additionally, the Lombardi CVT model is applied to simulate mobility decline. This complete mobility model accounts for degradation owing to transverse acoustic phonon scattering, surface roughness scattering at the oxide interface, and scattering produced by vertical electric fields. This is crucial for biosensors

as the surface contact quality can dramatically effect sensitivity [26]. Finally, Fermi-Dirac statistics are activated to adequately describe carrier distribution in the highly doped source (10^{20} cm^{-3}) and drain regions, where the simpler Boltzmann approximation becomes inappropriate.

3.3 Fabrication Process Flow

The suggested fabrication process flow is given in Fig. 3.2 and employs a conventional CMOS-compatible flow, assuring the device may be produced employing current foundry capabilities.

A Silicon-On-Insulator (SOI) wafer is used to start the process **(a)**. In order to reduce parasitic leakage currents from the substrate and obtain superior electrical isolation, SOI technology is used. Next, asymmetric ion implantation is done to define the highly doped P-type Source and N-type Drain regions **(b)**, followed by rapid thermal annealing (RTA) for dopant activation.

A thin 3 nm InAs pocket layer is epitaxially grown at the source junction **(c)**. Indium Arsenide (InAs) has a shorter bandgap than Silicon, which considerably lowers the tunneling barrier width and enhances the on-current (I_{ON}) [27]. Step **(d)** involves creating a dual-thickness channel profile by a Reactive Ion Etch (RIE), which defines the sensing and control regions.

A High-κ dielectric layer (HfO_2) is then created using Atomic Layer Deposition (ALD) **(e)**. ALD is needed here to ensure conformal coverage of the sidewalls and a high-quality interface with minimum flaws [28]. The oxide is then shaped and etched **(f)** to reveal the sensing area where biomolecules will be attached.

To create the sensing void, a sacrificial layer (usually polysilicon or oxide) is placed **(g)** and etched back to form the nanocavity **(h)** near the source junction [14]. The metal gate electrode is placed using sputtering **(h)** over the control oxide. Isolation is obtained by etching the substrate from the backside using the Buried Oxide (BOX) layer as an etch-stop **(i)**. Finally, wafer bonding techniques for structural integration and contact metallization are completed **(j)** to construct the device terminals suitable for testing.

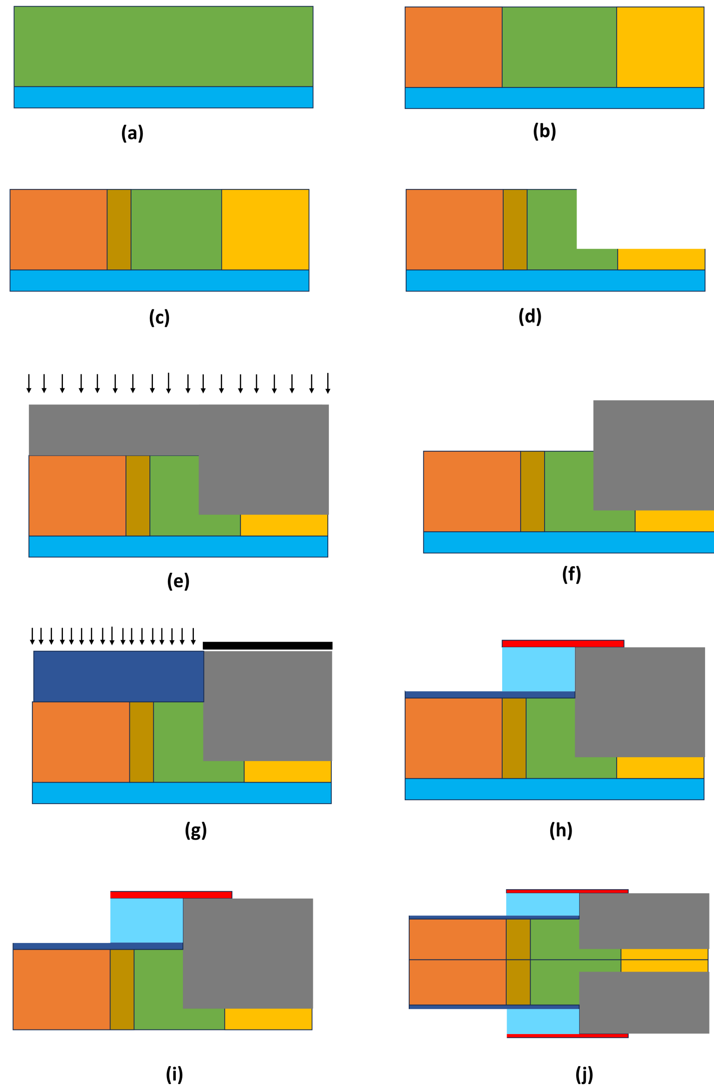

Figure 3.2: Proposed fabrication process flow for the TFET biosensor: (a) SOI Substrate Preparation; (b) Ion Implantation for Source/Drain; (c) Epitaxial Growth of InAs Pocket; (d) Channel Etching to define dual-thickness; (e) High-κ Dielectric Deposition; (f) Oxide Patterning; (g) Sacrificial material and Low-κ Deposition; (h) Sacrificial Etch for Nanocavity and Metal Gate Deposition; (i) Backside Etching; (j) Finalization, wafer bonding, and Contact Metallization.

Chapter 4

RESULTS AND DISCUSSION

The electrical characteristics of the suggested pocket-engineered DM-TFET are mainly determined by the dielectric properties of the biological materials within the nanocavity. Table 4.1 summarizes the specific breast cancer cell lines and the healthy reference cell used in this simulation, along with their respective dielectric constants (k).

Table 4.1: Various Cell Lines with Corresponding Dielectric Constants (k)

Cell Line	Dielectric Constant (k)	Nature	Ref.
MCF-10A	4.5	Healthy Breast Cell	[8]
Hs578T	22.0	Cancer Cell	[8]
MDA-MB-231	24.5	Cancer Cell	[8]
MCF-7	27.5	Cancer Cell	[8]
T47D	32.0	Cancer Cell	[8]

4.1 DC Characteristics

The drain current monotonically increases with the dielectric constant of the immobilized cell. The air filled cavity exhibits the lowest current while the T47D cell exhibits the highest current owing to the strongest gate coupling, in agreement with literature [14].

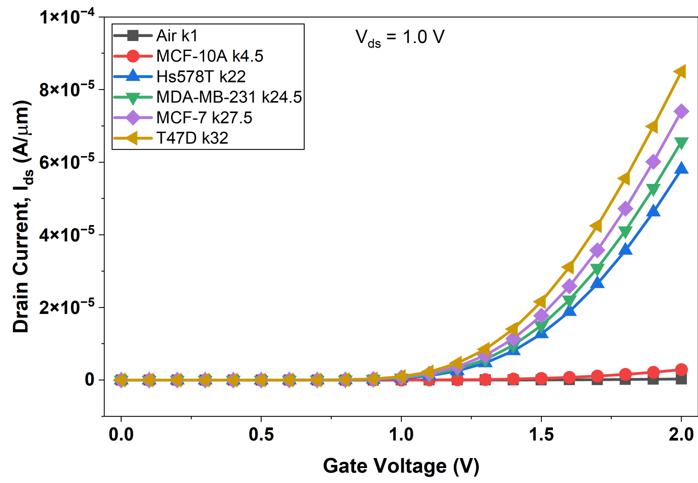

Figure 4.1: Drain current versus gate voltage linear plot I_{ds} vs. V_{gs}.

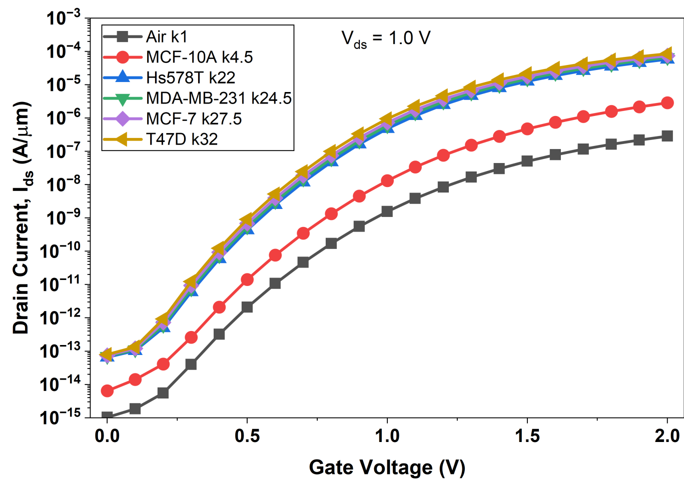

Figure 4.2: Logarithmic plot of Drain Current (I_{ds}) versus Gate Voltage (V_{gs}).

4.2 Surface Potential and Electric Field Analysis

Detection mechanism is electrostatic modulation. The surface potential along the channel is shown in Fig. 4.3. The potential curve is larger and steeper in the case of high dielectric malignant cells (T47D, $k = 32$) indicating more band bending compared to healthy cells.

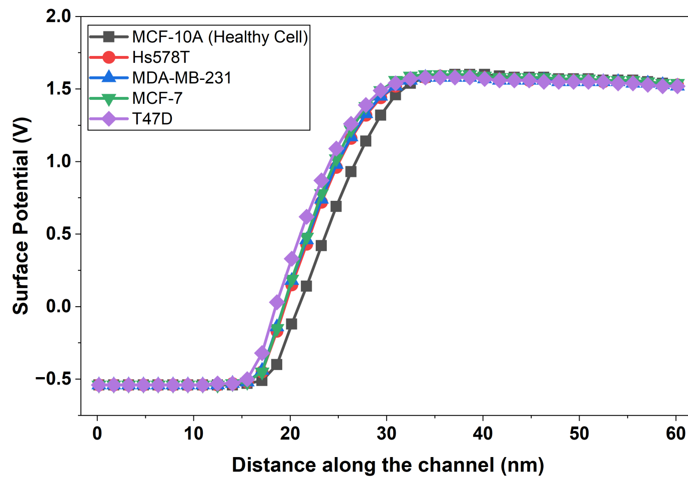

Figure 4.3: Surface potential variation along the channel length for different cell lines.

This gradient has an effect on the electric field (Fig. 4.4). The maximum electric field increases considerably for T47D cells to over 2.3×10^6 V/μm, favoring the tunneling rate through the BTBT mechanism [12].

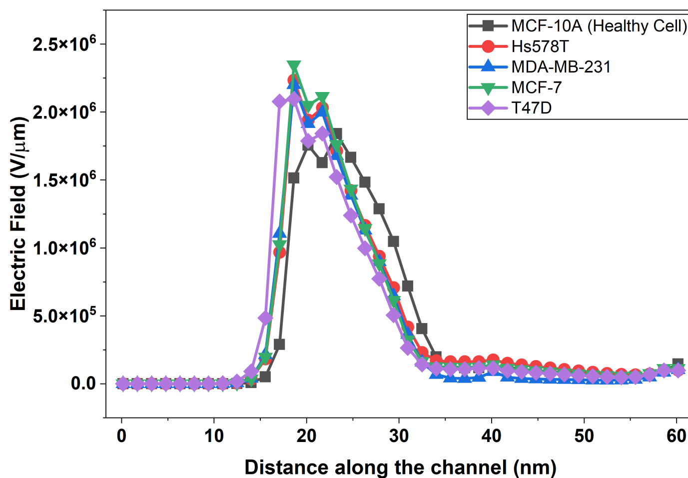

Figure 4.4: Distribution of electric field across the channel length.

4.3 Static & Dynamic Parameter Analysis

To measure the performance, we took static parameters (V_{th}, I_{ON}) and dynamic parameters (g_m, SS). Fig. 4.5 shows the Threshold Voltage (V_{th}) and On-Current (I_{ON}) as a function of cell type. The V_{th} is in a decreasing trend from 1.60 V (Healthy) to 1.44 V (T47D) while the I_{ON} increases, which means that the device is activated earlier and shows improved conductivity for malignant cells.

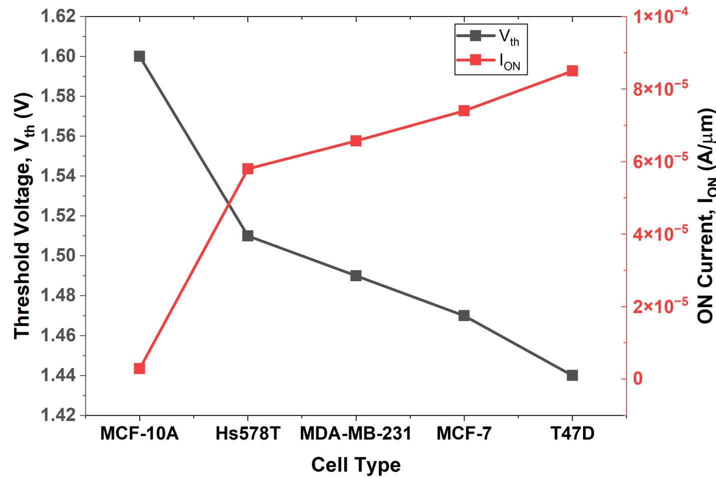

Figure 4.5: Threshold voltage (V_{th}) and on-state current (I_{ON}) variation with cell type.

Figure depicts transconductance (g_m) vs gate voltage for each cell line. 4.6. Compared to healthy cells, malignant cells show a rapid increase of g_m, with higher signal amplification capabilities [29].

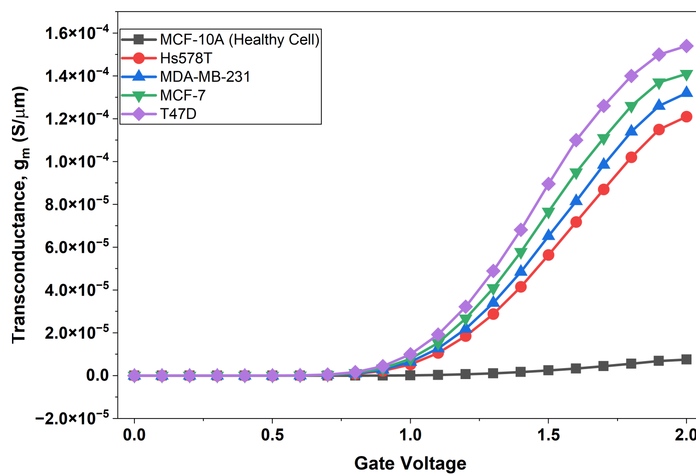

Figure 4.6: Gm (transconductance) vs. V_{gs} (gate voltage) for all the cell lines.

The peak g_m and Subthreshold Swing (SS) are shown in Fig. 4.7. The measured SS is 94.3 mV/dec for high-risk cells. While perfect TFETs can reach

sub-60 mV/dec, the integration of the sensing nanocavity naturally reduces gate coupling, resulting in a slightly larger SS. However, this value remains significantly superior to traditional MOSFET-based biosensors which typically exhibit $SS > 120$ mV/dec, guaranteeing that the proposed device maintains high sensitivity and distinct switching.

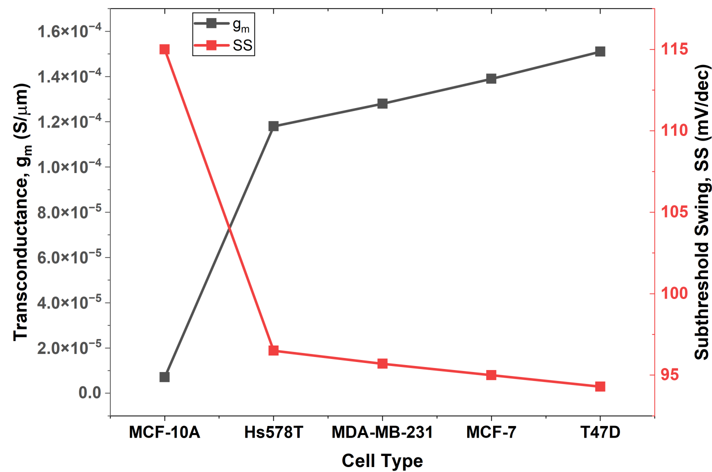

Figure 4.7: Peak Transconductance (g_m) and Subthreshold Swing (SS) obtained for each cell type.

4.4 Selectivity Analysis

Selectivity (S) is defined as the ratio of the drain current of the target cell to that of the healthy reference cell. As illustrated in Fig. 4.8, the proposed pocket-engineered DM-TFET demonstrates a remarkable selectivity profile. For the high-risk T47D cell line ($k = 32$) the device obtains a selectivity factor of 29.6. This means that the current signal generated by the cancer cells is roughly 30 times stronger than that of healthy cells. This significant margin is related to the nonlinear dependency of the tunneling probability on the gate capacitance. The high dielectric constant of malignant cells significantly raises the electric field at the source junction, dramatically enhancing the tunneling generation rate compared to the low-dielectric healthy cells. Such strong selectivity is crucial for early-stage diagnosis, because the concentration of malignant cells may be low relative to the background of healthy cells, providing a low false-positive rate and high diagnostic confidence.

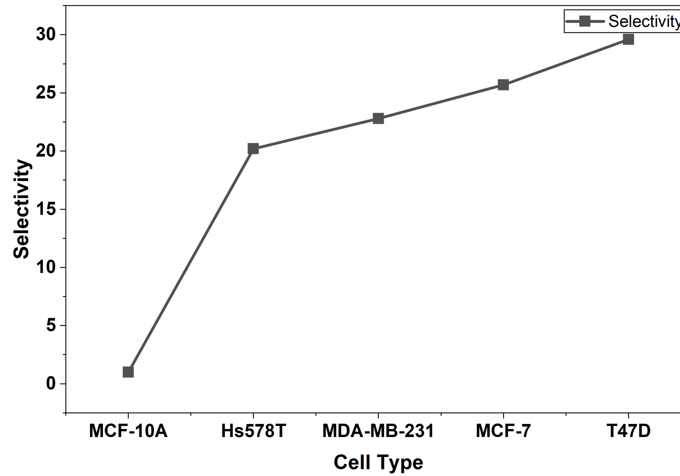

Figure 4.8: Selectivity of the biosensor normalized to the healthy MCF-10A cell.

4.5 Sensitivity Analysis

The sensitivity of the proposed biosensor for cancer detection is determined using the standard expression:

$$S(x) = \frac{x_{bio} - x_{air}}{x_{air}} \tag{4.1}$$

Where x is the computed sensitivity electrical parameter (such as I_{ds}, V_{th}, or g_m), x_{bio} is the electrical parameter measured when the cavity is filled with the specific cancer cell line, and x_{air} is the electrical parameter when the cavity is empty.

4.5.1 Threshold Voltage Sensitivity (ΔV_{th})

The absolute change in threshold voltage with respect to the air-filled cavity is known as the threshold voltage sensitivity:

$$\Delta V_{th} = V_{th(air)} - V_{th(bio)} \tag{4.2}$$

where $V_{th(air)}$ is the threshold voltage when there is air in the cavity and $V_{th(bio)}$ is the threshold voltage when there is a biomolecule present. As the dielectric constant increases, sensitivity steadily increases, as seen in Fig. 4.9. For example, the shift is small in healthy MCF-10A cells ($k = 4.5$). For high-risk T47D cells ($k = 32$), the device's maximal sensitivity is 130 mV. This significant shift is useful for real-world sensing applications as it produces a distinct, quantifiable signal that is resistant to noise and exceeds the sensitivity levels seen in similar doping-less TFET devices [29].

4.5.2 Sensitivities of Drain Currents (SIDs)

The drain current sensitivity is calculated using $x = I_{\text{ds}}$ in Eq. 4.1. Fig. 4.10 shows S_{Ids} reaching a maximum of 606 for T47D cells at $V_{\text{gs}} = 1.0$ V. The explicit

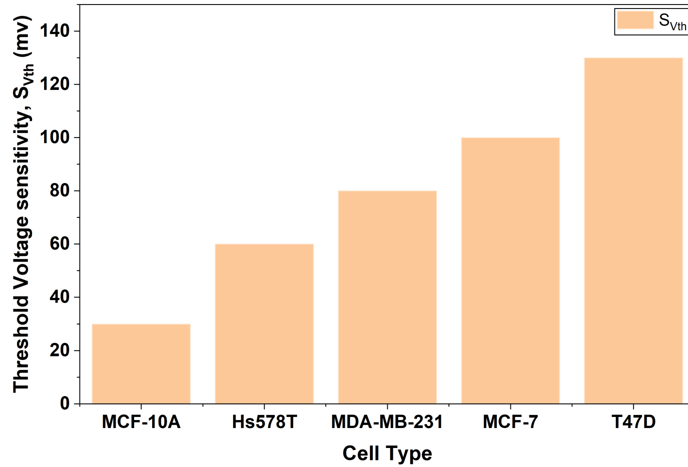

Figure 4.9: Fig. 4.9. Sensitivity of the Threshold Voltage (ΔV_{th}) with respect to Air.

computation is:

$$S_{Ids} = \frac{I_{ds(bio)} - I_{ds(air)}}{I_{ds(air)}} \tag{4.3}$$

Fig. 4.11 shows strong sensitivity ($S_{\text{Ion}} \approx 297$) even for high gate voltages ($V_{\text{gs}} = 2.0$ V), which indicates the substantial slope advantage of the TFET [8].

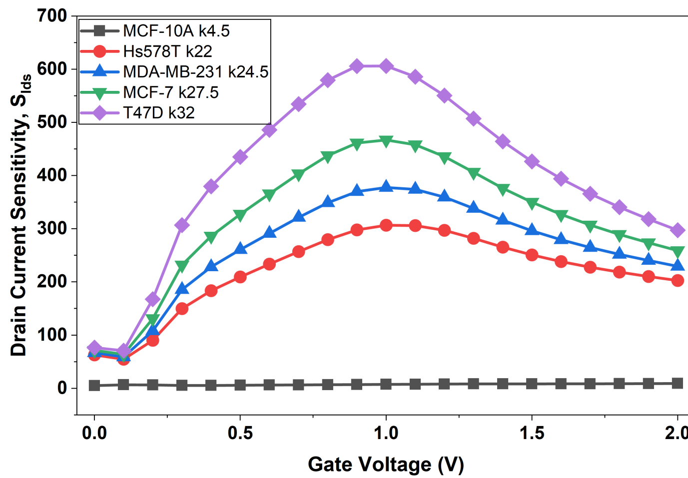

Figure 4.10: Drain Current Sensitivity (S_{Ids}) versus Gate Voltage.

Furthermore, a huge dynamic sensitivity (S_{gm}) of 228 is seen in Fig. 4.12. Transconductance sensitivity is a critical figure of merit for analog sensing applications as it measures the shift in the device's capability for amplification after the immobilization of biomolecules. This high result demonstrates that the presence of T47D cancer cells ($k = 32$) not only shifts the threshold voltage but also greatly enhances the gate control efficiency across the channel. Consequently, even minute changes in the biomolecule concentration may be detected as large variances in

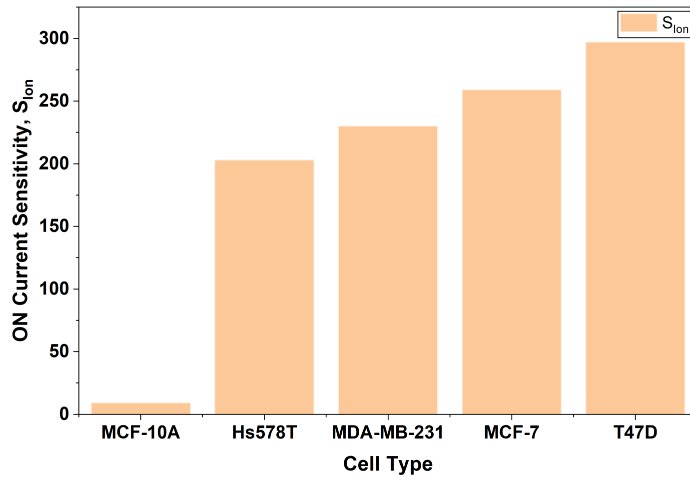

Figure 4.11: ON-Current Sensitivity (S_{Ion}) at $V_{gs} = 2.0$ V.

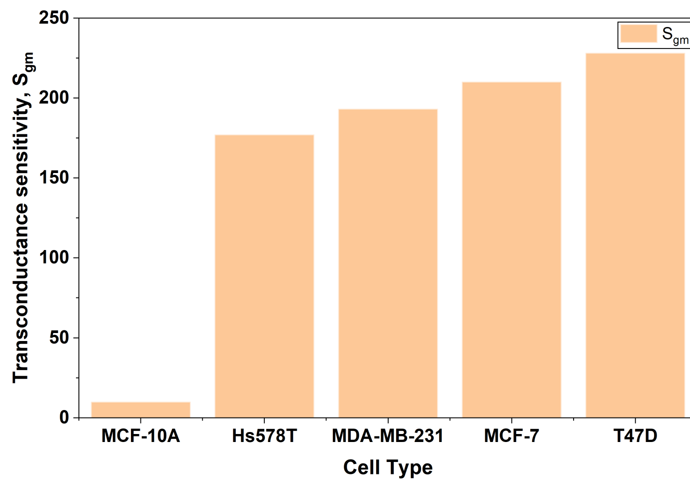

Figure 4.12: Transconductance Sensitivity (S_{gm}) relative to Air.

the device's switching speed, affording a unique advantage over standard sensors that depend only on static current shifts.

4.6 Impact of Biomolecule Occupancy

Because of steric barrier, surface roughness, or the random orientation of biomolecules during the immobilization process, it could be problematic to guarantee 100% filling of the nanocavity in real-world biological sensing conditions. Therefore, studying the sensor's responsiveness under partial filling situations is crucial for assessing its resilience and reliability in real-world applications. We simulated the nanocavity's fill factor for both malignant (T47D) and healthy (MCF-10A) cell lines at different intervals, such as 25%, 50%, 75%, and 100%.

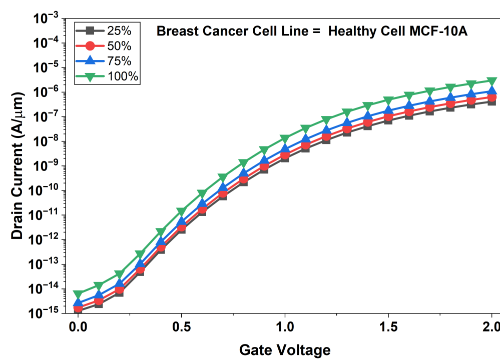

Figure 4.13: Impact of occupancy on transfer characteristics for healthy MCF-10A cells.

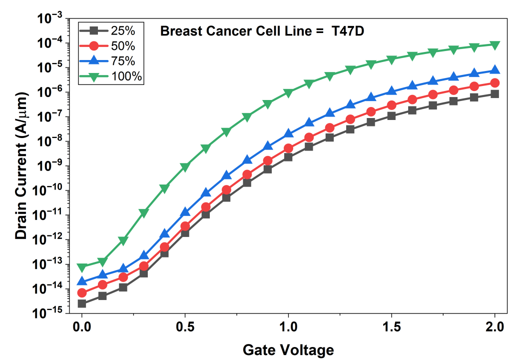

Figure 4.14: Impact of occupancy on transfer characteristics for high-risk T47D cells.

The transfer characteristics for healthy MCF-10A cells are shown in Fig. 4.13. As the occupancy increases, the drain current displays a marginal amplification, about 7 times at full occupancy. This very tiny gain is owing to the lower dielectric constant ($k = 4.5$) of the healthy cells, which offers only a limited improvement in gate coupling.

Fig. 4.14, on the other hand, shows the effect of occupancy for the high-risk T47D cancer cells ($k = 32$). Here the drain current exhibits a huge surge, increasing by almost two orders of magnitude ($>$ 100-times) as the cavity fills. The high dielectric constant of the malignant cells considerably increases the gate oxide capacitance (C_{ox}) which drastically narrows the tunneling barrier width at the source-channel interface. This non-linear, exponential increase of the tunneling probability with occupancy indicates that the sensor is very sensitive to the volume of malignant biological material present. The sensor shows a clear and distinct change in signal at 40–60 % occupancy, which means that detection of high risk cancer cells will not be affected by partial filling.

Fig. 4.15 shows the static parameter shifts. As the increase of the occupancy, the threshold voltage (V_{th}) for cancer cells reduces quickly from 1.62 V to 1.44 V, which indicates the switching properties change a lot. On the other hand, healthy

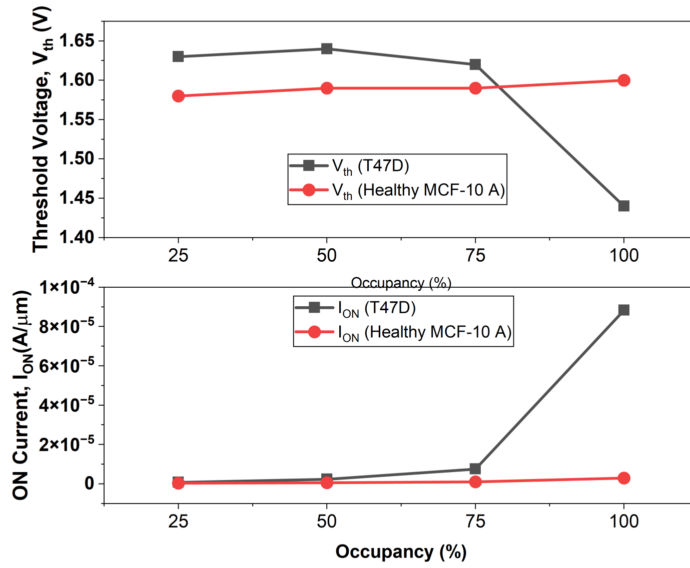

Figure 4.15: Vth and I_{ION} versus occupancy for MCF-10A vs. T47D.

cells have a rather stable V_{th}, which means only a small change. The diagnostic accuracy and the chances of false positives are minimized by the unique electrical responses of healthy and malignant cells even at different occupancy levels.

4.7 Performance Evaluation

The performance of the proposed device is compared with the previously reported TFET based biosensors as shown in Table 4.2. As can be seen from the table, this work has a current sensitivity (S_{Ion}) of 2.97×10^2 and threshold voltage shift (ΔV_{th}) of 130 mV. These values are higher than those reported for the other devices in the comparison.

Table 4.2: Benchmark Comparison: TFET Biosensor Sensitivity

Biosensors	S_{ion}	ΔV_{th} **(mV)**
Ref. [8]	1.1×10^2	–
Ref. [29] (I)	1×10^1	66
Ref. [29] (II)	4×10^1	54
Ref. [30]	2.5×10^2	–
This Work	$\mathbf{2.97 \times 10^2}$	**130**

Chapter 5

CONCLUSION, FUTURE SCOPE AND SOCIAL IMPACT

5.1 Summary of Key Research Findings

This study describes the design and simulation of a pocket-engineered DM-TFET for label-free breast cancer detection. The device exhibits sharper switching behavior than conventional MOSFET-based biosensors. This improvement is achieved by adding a nanocavity at the source-channel tunneling junction and using a hetero-material InAs pocket. The sensor is highly sensitive to changes in the dielectric permittivity of the immobilized cells.

Simulation results show that the device responds strongly to high-risk T47D cells, with a peak transconductance sensitivity of 228 and a peak drain current sensitivity of 606. The results also show that the sensor continues to perform well even when the biomolecule occupancy is partial rather than full. Another clear observation is that cancerous cells produce current spikes almost 100 times higher than those from healthy cells.

5.2 Future Scope and Social Impact

The clinical and social implications of this work are broad. By moving early cancer diagnostics away from invasive infrastructure and tracking shifts dynamically inside an electronic POC node, cost-barriers drop dramatically. Future engineering directives may analyze dynamic microfluidic integration alongside multi-target tracking cells to track multiple structural biomarkers simultaneously.

REFERENCES

[1] F. Bray, J. Ferlay, I. Soerjomataram, R. L. Siegel, L. A. Torre, A. Jemal, Global cancer statistics 2018: GLOBOCAN estimates of incidence and mortality worldwide for 36 cancers in 185 countries, CA: A Cancer J. Clin. 68 (2018) 394–424. https://doi.org/10.3322/caac.21492.

[2] R. L. Siegel, K. D. Miller, A. Jemal, Cancer statistics, 2018, CA: A Cancer J. Clin. 68 (2018) 7–30. https://doi.org/10.3322/caac.21442.

[3] World Health Organization, Breast cancer, Geneva, Switzerland, 2022. [Online]. Available: `https://www.who.int/news-room/fact-sheets/detail/breast-cancer`

[4] D. N. Elsheakh, O. M. Fahmy, M. Farouk, K. Ezzat, A. R. Eldamak, An early breast cancer detection by using wearable flexible sensors and artificial intelligent, IEEE Access 12 (2024) 48511–48529. https://doi.org/10.1109/ACCESS.2024.3380453.

[5] S. P. Mohanty, E. Kougianos, Biosensors: A Tutorial Review, IEEE Potentials 25 (2006) 35–40. https://doi.org/10.1109/MP.2006.1649009.

[6] A. Aminzadeh, et al., Imaging breast microcalcifications using dark-field signal in propagation-based phase-contrast tomography, IEEE Trans. Med. Imag. 41 (2022) 2980–2990. https://doi.org/10.1109/TMI.2022.3175924.

[7] P. Harika, G. S. Kondavitee, S. R. Karumuri, A. Lay-Ekuakille, High sensitivity of dielectrically modulated tunnel field effect transistor for biosensor applications, IEEE Trans. Nanobiosci. (2024). https://doi.org/10.1109/TNB.2024.3386586.

[8] P. Kaushal, G. Khanna, Breast Cancer Detection Using Si-Doped MoS2 Channel-Based Thickness Engineered TFET Biosensor, IEEE Sensors Lett. 8 (2024) 1–4. https://doi.org/10.1109/LSENS.2024.3438872.

[9] A. M. Ionescu, H. Riel, Tunnel field-effect transistors as energy-efficient electronic switches, Nature 479 (2011) 329–337. https://doi.org/10.1038/nature10679.

[10] J. Appenzeller, et al., Band-to-band tunneling in carbon nanotube field-effect transistors, Phys. Rev. Lett. 93 (2004) 196805. https://doi.org/10.1103/PhysRevLett.93.196805.

[11] T. Krishnamohan, et al., Double-Gate Strained-Ge Heterostructure Tunneling FET (TFET) With record high drive currents and $\leq$ 60mV/dec subthreshold slope, IEEE IEDM (2008). https://doi.org/10.1109/IEDM.2008.4796839.

[12] W. Y. Choi, et al., Tunneling Field-Effect Transistors (TFETs) with Subthreshold Swing (SS) Less Than 60 mV/dec, IEEE Electron Device Lett. 28 (2007) 743–745. https://doi.org/10.1109/LED.2007.901273.

[13] V. Thakur, A. Kumar, S. Kale, Analytical modeling of space engineered reconfigurable silicon nanowire Schottky barrier transistor for biosensing applications, Micro Nanostruct. 188 (2024) 207799. https://doi.org/10.1016/j.micrna.2024.207799.

[14] D. Sarkar, K. Banerjee, Proposal for a Tunnel-Field-Effect-Transistor-Based Dielectric-Modulated Biosensor, Appl. Phys. Lett. 100 (2012) 143108. https://doi.org/10.1063/1.3698093.

[15] C. Li, F. Liu, R. Han, Y. Zhuang, A vertically stacked nanosheet gate-all around FET for biosensing application, IEEE Access 9 (2021) 63602–63610. https://doi.org/10.1109/ACCESS.2021.3074906.

[16] K. Boucart, A. M. Ionescu, Double-Gate Tunnel FET With High-kappa Gate Dielectric, IEEE Trans. Electron Devices 54 (2007) 1725–1733. https://doi.org/10.1109/TED.2007.899389.

[17] S. M. Sze, K. K. Ng, Physics of Semiconductor Devices, 3rd ed., Wiley, 2006. https://doi.org/10.1002/0470068329.

[18] R. Vishnoi, M. J. Kumar, Compact Analytical Model of Dual Material Gate Tunneling Field-Effect Transistor Using Interband Tunneling and Channel Transport, IEEE Trans. Electron Devices 61 (2014) 1936–1942. https://doi.org/10.1109/TED.2014.2315294.

[19] S. R. Upadhyay, S. Kale, A. Pandey, Dielectric Modulated InAs Pocket Heterojunction tunnel FET for biosensor applications, ECS J. Solid State Sci. Technol. 14 (2025) 047006. https://doi.org/10.1149/2162-8777/adc338.

[20] K. N. Priyadarshani, S. Singh, Ultra sensitive breast cancer cell lines detection using dual nanocavities engraved junctionless FET, IEEE Trans. Nanobiosci. 22 (2023) 889–896. https://doi.org/10.1109/TNB.2023.3246106.

[21] R. Pethig, Dielectric and Electrical Properties of Biological Materials, J. Bioelectricity 4 (2009) vii–ix. https://doi.org/10.3109/15368378509033258.

[22] D. Barwa, D. Khanna, H. Parihar, S. Kale, A Novel n+ Pocket Doped L-Shaped Channel TFET for Biosensing Applications, ECS J. Solid State Sci. Technol. 14 (2025) 047010. https://doi.org/10.1149/2162-8777/adccf8.

[23] G. D. Wilk, et al., High-k gate dielectrics: Current status and materials properties considerations, J. Appl. Phys. 89 (2001) 5243–5275. https://doi.org/10.1063/1.1361065.

[24] M. Rahimian, M. Fathipour, Improvement of electrical performance in junctionless nanowire TFET using hetero-gate-dielectric, J. Mater. Sci. Semicond. Process. 63 (2017) 142–152. https://doi.org/10.1016/j.mssp.2016.12.011.

[25] A. C. Seabaugh, Q. Zhang, Low-Voltage Tunnel Transistors for Beyond CMOS Logic, Proc. IEEE 98 (2010) 2095–2110. https://doi.org/10.1109/JPROC.2010.2070470.

[26] C. Hu, Modern Semiconductor Devices for Integrated Circuits, Pearson, 2010.

[27] J. A. del Alamo, Nanometre-scale electronics with III-V compound semiconductors, Nature 479 (2011) 317–323. https://doi.org/10.1038/nature10677.

[28] M. Xiao, C. Qiu, Z. Zhang, L. M. Peng, Atomic-layer-deposition growth of an ultrathin HfO_2 film on graphene, ACS Applied Materials & Interfaces 9 (2017) 34050–34056. https://doi.org/10.1021/acsami.7b09408.

[29] S. Anand, A. Singh, S. I. Amin, A. S. Thool, Design and Performance Analysis of Dielectrically Modulated Doping-Less Tunnel FET-Based Label Free Biosensor, IEEE Sensors J. 19 (2019) 4369–4376. https://doi.org/10.1109/JSEN.2019.2900092.

[30] A. Bhattacharyya, M. Chanda, d. De, Performance Assessment of New Dual-Pocket Vertical Heterostructure Tunnel FET-Based Biosensor Considering Steric Hindrance Issue, IEEE Trans. Electron Devices (2019) 1–6. https://doi.org/10.1109/TED.2019.2928850.

LIST OF PUBLICATIONS

1. **Shishir Bhargav** and Sumit Kale, "Design and Simulation of a Pocket-Engineered Dielectric-Modulated TFET Biosensor for Label-Free Breast Cancer Detection," submitted to *Silicon*, Springer Nature, 2026.

APPENDIX A: SILVACO ATLAS SIMULATION SCRIPT

```
# ==========================================================================
# POCKET-ENGINEERED DIELECTRIC-MODULATED TFET BIOSENSOR SIMULATION DECK
# Project Dissertation: Evaluation of Breast Cancer Permittivity Sensitivity
# Target Biomolecules: Air (k=1.0), MCF-10A (k=4.5), Hs578T (k=22.0),
#                      MDA-MB-231 (k=24.5), MCF-7 (k=27.5), T47D (k=32.0)
# ==========================================================================

# --------------------------------------------------------------------------
# MODULE 1: INTERFACING BASELINE SIMULATION PROFILE (VACUUM CAVITY CONDITIONS)
# --------------------------------------------------------------------------
go atlas

# Setting fine spatial discretization limits for advanced nonlocal tunneling verification
mesh space.mult=1.0

# Precise X-mesh definition covering the 3nm InAs pocket and nanocavity coordinates
x.mesh loc=-0.002 spacing=0.001
x.mesh loc=0.000  spacing=0.001
x.mesh loc=0.015  spacing=0.001
x.mesh loc=0.020  spacing=0.00005
x.mesh loc=0.023  spacing=0.00005
x.mesh loc=0.031  spacing=0.0001
x.mesh loc=0.042  spacing=0.00005
x.mesh loc=0.062  spacing=0.001
x.mesh loc=0.064  spacing=0.001

# Y-mesh mesh distribution establishing thin spatial inversion layer grid
y.mesh loc=-0.002 spacing=0.001
y.mesh loc=0.000  spacing=0.001
y.mesh loc=0.005  spacing=0.0005
y.mesh loc=0.006  spacing=0.0002
y.mesh loc=0.011  spacing=0.0005
y.mesh loc=0.016  spacing=0.001
y.mesh loc=0.021  spacing=0.0005
y.mesh loc=0.027  spacing=0.001
y.mesh loc=0.029  spacing=0.001

# Sub-surface quantum meshing configuration grid across source-channel interface
qtx.mesh loc=0.015 spac=2.5e-4
qtx.mesh loc=0.020 spac=5.0e-5
```

```
qtx.mesh loc=0.023 spac=5.0e-5
qtx.mesh loc=0.031 spac=1.0e-4
qtx.mesh loc=0.042 spac=5.0e-5
qtx.mesh loc=0.047 spac=2.5e-4

qty.mesh loc=0.006 spac=5.0e-4
qty.mesh loc=0.011 spac=2.0e-4
qty.mesh loc=0.013 spac=2.0e-4
qty.mesh loc=0.014 spac=2.0e-4
qty.mesh loc=0.016 spac=5.0e-4
qty.mesh loc=0.021 spac=5.0e-4

# Structuring device layers: bulk silicon, high-k drain oxide, and low-k source oxide
region num=1 material=Air       x.min=-0.002 x.max=0.064 y.min=-0.002 y.max=0.029
region num=2 material=Silicon   x.min=0.000  x.max=0.062 y.min=0.006  y.max=0.021
region num=11 material=InAs     x.min=0.020  x.max=0.023 y.min=0.006  y.max=0.021
region num=3 material=Silicon   x.min=0.023  x.max=0.031 y.min=0.006  y.max=0.021
region num=10 material=Silicon  x.min=0.031  x.max=0.042 y.min=0.011  y.max=0.016
region num=4 material=HfO2      x.min=0.031  x.max=0.062 y.min=0.000  y.max=0.011
region num=5 material=SiO2      x.min=0.000  x.max=0.031 y.min=0.005  y.max=0.006
region num=6 material=SiO2      x.min=0.000  x.max=0.031 y.min=0.021  y.max=0.022
region num=7 material=HfO2      x.min=0.031  x.max=0.062 y.min=0.016  y.max=0.027

# Defining the dual-nanocavity sensing voids mapping to the geometry
region num=8 user.material=cavity x.min=0.020 x.max=0.031 y.min=0.000 y.max=0.005
region num=9 user.material=cavity x.min=0.020 x.max=0.031 y.min=0.022 y.max=0.027

# Attaching terminal electrode configurations
electrode name=gate  x.min=0.020 x.max=0.042 y.min=-0.001 y.max=0.000
electrode name=gate2 x.min=0.020 x.max=0.042 y.min=0.027  y.max=0.028
electrode name=source x.min=-0.002 x.max=0.000 y.min=0.006 y.max=0.021
electrode name=drain  x.min=0.062  x.max=0.064 y.min=0.011 y.max=0.016

# Mapping the asymmetric doping concentrations matching device architecture
doping uniform p.type conc=1e20 x.min=0.000 x.max=0.020 y.min=0.006 y.max=0.021
doping uniform n.type conc=1e18 x.min=0.042 x.max=0.062 y.min=0.011 y.max=0.016
doping uniform n.type conc=1e12 x.min=0.020 x.max=0.031 y.min=0.006 y.max=0.021
doping uniform n.type conc=1e12 x.min=0.031 x.max=0.042 y.min=0.006 y.max=0.021

# Initializing vacuum baseline conditions inside the variable cavity space
material material=cavity user.group=insulator user.default=oxide permittivity=1.0

# Setting target contact metal work functions
contact name=gate work=4.1
contact name=gate2 work=4.1 common=gate
contact name=source
contact name=drain

# Calibrating transport models: Nonlocal BTBT, Lombardi CVT, SRH, and Fermi Dirac
models srh boltzmann fermi cvt bgn bbt.nonlocal qtunn.dir=xdir

# Setting up custom high-convergence solver convergence criteria
method newton trap maxtraps=50
output p.quantum band.temp con.band val.band band.par
```

```
solve init
solve vdrain=1.0 name=drain
log outf="Air_K1.log"
solve vgate=0.0 name=gate vstep=0.1 vfinal=2.0
log off
save outf="Air_K1.str"

# Mathematical extraction statements logging baseline DC figures of merit
extract init infile="Air_K1.log"
extract name="vt1_Air" (xintercept(maxslope(curve(v."gate",i."drain"))))
extract name="Ion_Air" (max(abs(i."drain")))
extract name="Ioff_Air" (min(abs(i."drain")))
extract name="Ratio_Air" ((max(abs(i."drain")))/(min(abs(i."drain"))))
extract name="gm_Air" (slope(maxslope(curve(abs(v."gate"),abs(i."drain")))))


# -------------------------------------------------------------------------
# MODULE 2: EVALUATION OF HEALTHY MCF-10A RECEPTOR LOADINGS (k = 4.5)
# -------------------------------------------------------------------------
go atlas

mesh space.mult=1.0

x.mesh loc=-0.002 spacing=0.001
x.mesh loc=0.000  spacing=0.001
x.mesh loc=0.015  spacing=0.001
x.mesh loc=0.020  spacing=0.00005
x.mesh loc=0.023  spacing=0.00005
x.mesh loc=0.031  spacing=0.0001
x.mesh loc=0.042  spacing=0.00005
x.mesh loc=0.062  spacing=0.001
x.mesh loc=0.064  spacing=0.001

y.mesh loc=-0.002 spacing=0.001
y.mesh loc=0.000  spacing=0.001
y.mesh loc=0.005  spacing=0.0005
y.mesh loc=0.006  spacing=0.0002
y.mesh loc=0.011  spacing=0.0005
y.mesh loc=0.016  spacing=0.001
y.mesh loc=0.021  spacing=0.0005
y.mesh loc=0.027  spacing=0.001
y.mesh loc=0.029  spacing=0.001

qtx.mesh loc=0.015 spac=2.5e-4
qtx.mesh loc=0.020 spac=5.0e-5
qtx.mesh loc=0.023 spac=5.0e-5
qtx.mesh loc=0.031 spac=1.0e-4
qtx.mesh loc=0.042 spac=5.0e-5
qtx.mesh loc=0.047 spac=2.5e-4

qty.mesh loc=0.006 spac=5.0e-4
qty.mesh loc=0.011 spac=2.0e-4
qty.mesh loc=0.013 spac=2.0e-4
qty.mesh loc=0.014 spac=2.0e-4
qty.mesh loc=0.016 spac=5.0e-4
```

```
qty.mesh loc=0.021 spac=5.0e-4

region num=1 material=Air       x.min=-0.002 x.max=0.064 y.min=-0.002 y.max=0.029
region num=2 material=Silicon   x.min=0.000  x.max=0.062 y.min=0.006  y.max=0.021
region num=11 material=InAs     x.min=0.020  x.max=0.023 y.min=0.006  y.max=0.021
region num=3 material=Silicon   x.min=0.023  x.max=0.031 y.min=0.006  y.max=0.021
region num=10 material=Silicon  x.min=0.031  x.max=0.042 y.min=0.011  y.max=0.016
region num=4 material=HfO2      x.min=0.031  x.max=0.062 y.min=0.000  y.max=0.011
region num=5 material=SiO2      x.min=0.000  x.max=0.031 y.min=0.005  y.max=0.006
region num=6 material=SiO2      x.min=0.000  x.max=0.031 y.min=0.021  y.max=0.022
region num=7 material=HfO2      x.min=0.031  x.max=0.062 y.min=0.016  y.max=0.027

region num=8 user.material=cavity x.min=0.020 x.max=0.031 y.min=0.000 y.max=0.005
region num=9 user.material=cavity x.min=0.020 x.max=0.031 y.min=0.022 y.max=0.027

electrode name=gate  x.min=0.020 x.max=0.042 y.min=-0.001 y.max=0.000
electrode name=gate2 x.min=0.020 x.max=0.042 y.min=0.027  y.max=0.028
electrode name=source x.min=-0.002 x.max=0.000 y.min=0.006 y.max=0.021
electrode name=drain  x.min=0.062  x.max=0.064 y.min=0.011 y.max=0.016

doping uniform p.type conc=1e20 x.min=0.000 x.max=0.020 y.min=0.006 y.max=0.021
doping uniform n.type conc=1e18 x.min=0.042 x.max=0.062 y.min=0.011 y.max=0.016
doping uniform n.type conc=1e12 x.min=0.020 x.max=0.031 y.min=0.006 y.max=0.021
doping uniform n.type conc=1e12 x.min=0.031 x.max=0.042 y.min=0.006 y.max=0.021

# Adjusting permittivity factor mapping to standard MCF-10A biological structures
material material=cavity user.group=insulator user.default=oxide permittivity=4.5

contact name=gate work=4.1
contact name=gate2 work=4.1 common=gate
contact name=source
contact name=drain

models srh boltzmann fermi cvt bgn bbt.nonlocal qtunn.dir=xdir

method newton trap maxtraps=50
output p.quantum band.temp con.band val.band band.par

solve init
solve vdrain=1.0 name=drain
log outf="MCF10A_K4.5.log"
solve vgate=0.0 name=gate vstep=0.1 vfinal=2.0
log off
save outf="MCF10A_K4.5.str"

extract init infile="MCF10A_K4.5.log"
extract name="vt1_MCF10A" (xintercept(maxslope(curve(v."gate",i."drain"))))
extract name="Ion_MCF10A" (max(abs(i."drain")))
extract name="Ioff_MCF10A" (min(abs(i."drain")))
extract name="Ratio_MCF10A" ((max(abs(i."drain")))/(min(abs(i."drain"))))
extract name="gm_MCF10A" (slope(maxslope(curve(abs(v."gate"),abs(i."drain")))))


# -------------------------------------------------------------------------
# MODULE 3: CHARACTERIZING MALIGNANT Hs578T VARIANT IMMOBILIZATION (k = 22.0)
```

```
# ---------------------------------------------------------------------------
go atlas

mesh space.mult=1.0

x.mesh loc=-0.002 spacing=0.001
x.mesh loc=0.000  spacing=0.001
x.mesh loc=0.015  spacing=0.001
x.mesh loc=0.020  spacing=0.00005
x.mesh loc=0.023  spacing=0.00005
x.mesh loc=0.031  spacing=0.0001
x.mesh loc=0.042  spacing=0.00005
x.mesh loc=0.062  spacing=0.001
x.mesh loc=0.064  spacing=0.001

y.mesh loc=-0.002 spacing=0.001
y.mesh loc=0.000  spacing=0.001
y.mesh loc=0.005  spacing=0.0005
y.mesh loc=0.006  spacing=0.0002
y.mesh loc=0.011  spacing=0.0005
y.mesh loc=0.016  spacing=0.001
y.mesh loc=0.021  spacing=0.0005
y.mesh loc=0.027  spacing=0.001
y.mesh loc=0.029  spacing=0.001

qtx.mesh loc=0.015 spac=2.5e-4
qtx.mesh loc=0.020 spac=5.0e-5
qtx.mesh loc=0.023 spac=5.0e-5
qtx.mesh loc=0.031 spac=1.0e-4
qtx.mesh loc=0.042 spac=5.0e-5
qtx.mesh loc=0.047 spac=2.5e-4

qty.mesh loc=0.006 spac=5.0e-4
qty.mesh loc=0.011 spac=2.0e-4
qty.mesh loc=0.013 spac=2.0e-4
qty.mesh loc=0.014 spac=2.0e-4
qty.mesh loc=0.016 spac=5.0e-4
qty.mesh loc=0.021 spac=5.0e-4

region num=1 material=Air       x.min=-0.002 x.max=0.064 y.min=-0.002 y.max=0.029
region num=2 material=Silicon   x.min=0.000  x.max=0.062 y.min=0.006  y.max=0.021
region num=11 material=InAs     x.min=0.020  x.max=0.023 y.min=0.006  y.max=0.021
region num=3 material=Silicon   x.min=0.023  x.max=0.031 y.min=0.006  y.max=0.021
region num=10 material=Silicon  x.min=0.031  x.max=0.042 y.min=0.011  y.max=0.016
region num=4 material=HfO2      x.min=0.031  x.max=0.062 y.min=0.000  y.max=0.011
region num=5 material=SiO2      x.min=0.000  x.max=0.031 y.min=0.005  y.max=0.006
region num=6 material=SiO2      x.min=0.000  x.max=0.031 y.min=0.021  y.max=0.022
region num=7 material=HfO2      x.min=0.031  x.max=0.062 y.min=0.016  y.max=0.027

region num=8 user.material=cavity x.min=0.020 x.max=0.031 y.min=0.000 y.max=0.005
region num=9 user.material=cavity x.min=0.020 x.max=0.031 y.min=0.022 y.max=0.027

electrode name=gate  x.min=0.020 x.max=0.042 y.min=-0.001 y.max=0.000
electrode name=gate2 x.min=0.020 x.max=0.042 y.min=0.027  y.max=0.028
electrode name=source x.min=-0.002 x.max=0.000 y.min=0.006 y.max=0.021
```

```
electrode name=drain  x.min=0.062  x.max=0.064 y.min=0.011 y.max=0.016

doping uniform p.type conc=1e20 x.min=0.000 x.max=0.020 y.min=0.006 y.max=0.021
doping uniform n.type conc=1e18 x.min=0.042 x.max=0.062 y.min=0.011 y.max=0.016
doping uniform n.type conc=1e12 x.min=0.020 x.max=0.031 y.min=0.006 y.max=0.021
doping uniform n.type conc=1e12 x.min=0.031 x.max=0.042 y.min=0.006 y.max=0.021

# Mapping localized electrostatic field changes generated by Hs578T cells
material material=cavity user.group=insulator user.default=oxide permittivity=22.0

contact name=gate work=4.1
contact name=gate2 work=4.1 common=gate
contact name=source
contact name=drain

models srh boltzmann fermi cvt bgn bbt.nonlocal qtunn.dir=xdir

method newton trap maxtraps=50
output p.quantum band.temp con.band val.band band.par

solve init
solve vdrain=1.0 name=drain
log outf="Hs578T_K22.log"
solve vgate=0.0 name=gate vstep=0.1 vfinal=2.0
log off
save outf="Hs578T_K22.str"

extract init infile="Hs578T_K22.log"
extract name="vt1_Hs578T" (xintercept(maxslope(curve(v."gate",i."drain"))))
extract name="Ion_Hs578T" (max(abs(i."drain")))
extract name="Ioff_Hs578T" (min(abs(i."drain")))
extract name="Ratio_Hs578T" ((max(abs(i."drain")))/(min(abs(i."drain"))))
extract name="gm_Hs578T" (slope(maxslope(curve(abs(v."gate"),abs(i."drain")))))


# -------------------------------------------------------------------------
# MODULE 4: TRACKING MALIGNANT MDA-MB-231 TARGET PHENOTYPES (k = 24.5)
# -------------------------------------------------------------------------
go atlas

mesh space.mult=1.0

x.mesh loc=-0.002 spacing=0.001
x.mesh loc=0.000  spacing=0.001
x.mesh loc=0.015  spacing=0.001
x.mesh loc=0.020  spacing=0.00005
x.mesh loc=0.023  spacing=0.00005
x.mesh loc=0.031  spacing=0.0001
x.mesh loc=0.042  spacing=0.00005
x.mesh loc=0.062  spacing=0.001
x.mesh loc=0.064  spacing=0.001

y.mesh loc=-0.002 spacing=0.001
y.mesh loc=0.000  spacing=0.001
y.mesh loc=0.005  spacing=0.0005
```

```
y.mesh loc=0.006  spacing=0.0002
y.mesh loc=0.011  spacing=0.0005
y.mesh loc=0.016  spacing=0.001
y.mesh loc=0.021  spacing=0.0005
y.mesh loc=0.027  spacing=0.001
y.mesh loc=0.029  spacing=0.001

qtx.mesh loc=0.015 spac=2.5e-4
qtx.mesh loc=0.020 spac=5.0e-5
qtx.mesh loc=0.023 spac=5.0e-5
qtx.mesh loc=0.031 spac=1.0e-4
qtx.mesh loc=0.042 spac=5.0e-5
qtx.mesh loc=0.047 spac=2.5e-4

qty.mesh loc=0.006 spac=5.0e-4
qty.mesh loc=0.011 spac=2.0e-4
qty.mesh loc=0.013 spac=2.0e-4
qty.mesh loc=0.014 spac=2.0e-4
qty.mesh loc=0.016 spac=5.0e-4
qty.mesh loc=0.021 spac=5.0e-4

region num=1 material=Air       x.min=-0.002 x.max=0.064 y.min=-0.002 y.max=0.029
region num=2 material=Silicon   x.min=0.000  x.max=0.062 y.min=0.006  y.max=0.021
region num=11 material=InAs     x.min=0.020  x.max=0.023 y.min=0.006  y.max=0.021
region num=3 material=Silicon   x.min=0.023  x.max=0.031 y.min=0.006  y.max=0.021
region num=10 material=Silicon  x.min=0.031  x.max=0.042 y.min=0.011  y.max=0.016
region num=4 material=HfO2      x.min=0.031  x.max=0.062 y.min=0.000  y.max=0.011
region num=5 material=SiO2      x.min=0.000  x.max=0.031 y.min=0.005  y.max=0.006
region num=6 material=SiO2      x.min=0.000  x.max=0.031 y.min=0.021  y.max=0.022
region num=7 material=HfO2      x.min=0.031  x.max=0.062 y.min=0.016  y.max=0.027

region num=8 user.material=cavity x.min=0.020 x.max=0.031 y.min=0.000 y.max=0.005
region num=9 user.material=cavity x.min=0.020 x.max=0.031 y.min=0.022 y.max=0.027

electrode name=gate  x.min=0.020 x.max=0.042 y.min=-0.001 y.max=0.000
electrode name=gate2 x.min=0.020 x.max=0.042 y.min=0.027  y.max=0.028
electrode name=source x.min=-0.002 x.max=0.000 y.min=0.006 y.max=0.021
electrode name=drain  x.min=0.062  x.max=0.064 y.min=0.011 y.max=0.016

doping uniform p.type conc=1e20 x.min=0.000 x.max=0.020 y.min=0.006 y.max=0.021
doping uniform n.type conc=1e18 x.min=0.042 x.max=0.062 y.min=0.011 y.max=0.016
doping uniform n.type conc=1e12 x.min=0.020 x.max=0.031 y.min=0.006 y.max=0.021
doping uniform n.type conc=1e12 x.min=0.031 x.max=0.042 y.min=0.006 y.max=0.021

# Assembling correct calibrated relative permittivity assignments based on clinical guidelin
material material=cavity user.group=insulator user.default=oxide permittivity=24.5

contact name=gate work=4.1
contact name=gate2 work=4.1 common=gate
contact name=source
contact name=drain

models srh boltzmann fermi cvt bgn bbt.nonlocal qtunn.dir=xdir

method newton trap maxtraps=50
```

```
output p.quantum band.temp con.band val.band band.par

solve init
solve vdrain=1.0 name=drain
log outf="MDA_K24.5.log"
solve vgate=0.0 name=gate vstep=0.1 vfinal=2.0
log off
save outf="MDA_K24.5.str"

extract init infile="MDA_K24.5.log"
extract name="vt1_MDA" (xintercept(maxslope(curve(v."gate",i."drain"))))
extract name="Ion_MDA" (max(abs(i."drain")))
extract name="Ioff_MDA" (min(abs(i."drain")))
extract name="Ratio_MDA" ((max(abs(i."drain")))/(min(abs(i."drain"))))
extract name="gm_MDA" (slope(maxslope(curve(abs(v."gate"),abs(i."drain")))))


# ------------------------------------------------------------------------
# MODULE 5: PROFILE RUN OVER MALIGNANT MCF-7 STRAINS (k = 27.5)
# ------------------------------------------------------------------------
go atlas

mesh space.mult=1.0

x.mesh loc=-0.002 spacing=0.001
x.mesh loc=0.000  spacing=0.001
x.mesh loc=0.015  spacing=0.001
x.mesh loc=0.020  spacing=0.00005
x.mesh loc=0.023  spacing=0.00005
x.mesh loc=0.031  spacing=0.0001
x.mesh loc=0.042  spacing=0.00005
x.mesh loc=0.062  spacing=0.001
x.mesh loc=0.064  spacing=0.001

y.mesh loc=-0.002 spacing=0.001
y.mesh loc=0.000  spacing=0.001
y.mesh loc=0.005  spacing=0.0005
y.mesh loc=0.006  spacing=0.0002
y.mesh loc=0.011  spacing=0.0005
y.mesh loc=0.016  spacing=0.001
y.mesh loc=0.021  spacing=0.0005
y.mesh loc=0.027  spacing=0.001
y.mesh loc=0.029  spacing=0.001

qtx.mesh loc=0.015 spac=2.5e-4
qtx.mesh loc=0.020 spac=5.0e-5
qtx.mesh loc=0.023 spac=5.0e-5
qtx.mesh loc=0.031 spac=1.0e-4
qtx.mesh loc=0.042 spac=5.0e-5
qtx.mesh loc=0.047 spac=2.5e-4

qty.mesh loc=0.006 spac=5.0e-4
qty.mesh loc=0.011 spac=2.0e-4
qty.mesh loc=0.013 spac=2.0e-4
qty.mesh loc=0.014 spac=2.0e-4
```

```
qty.mesh loc=0.016 spac=5.0e-4
qty.mesh loc=0.021 spac=5.0e-4

region num=1 material=Air       x.min=-0.002 x.max=0.064 y.min=-0.002 y.max=0.029
region num=2 material=Silicon   x.min=0.000  x.max=0.062 y.min=0.006  y.max=0.021
region num=11 material=InAs     x.min=0.020  x.max=0.023 y.min=0.006  y.max=0.021
region num=3 material=Silicon   x.min=0.023  x.max=0.031 y.min=0.006  y.max=0.021
region num=10 material=Silicon  x.min=0.031  x.max=0.042 y.min=0.011  y.max=0.016
region num=4 material=HfO2      x.min=0.031  x.max=0.062 y.min=0.000  y.max=0.011
region num=5 material=SiO2      x.min=0.000  x.max=0.031 y.min=0.005  y.max=0.006
region num=6 material=SiO2      x.min=0.000  x.max=0.031 y.min=0.021  y.max=0.022
region num=7 material=HfO2      x.min=0.031  x.max=0.062 y.min=0.016  y.max=0.027

region num=8 user.material=cavity x.min=0.020 x.max=0.031 y.min=0.000 y.max=0.005
region num=9 user.material=cavity x.min=0.020 x.max=0.031 y.min=0.022 y.max=0.027

electrode name=gate  x.min=0.020 x.max=0.042 y.min=-0.001 y.max=0.000
electrode name=gate2 x.min=0.020 x.max=0.042 y.min=0.027  y.max=0.028
electrode name=source x.min=-0.002 x.max=0.000 y.min=0.006 y.max=0.021
electrode name=drain  x.min=0.062  x.max=0.064 y.min=0.011 y.max=0.016

doping uniform p.type conc=1e20 x.min=0.000 x.max=0.020 y.min=0.006 y.max=0.021
doping uniform n.type conc=1e18 x.min=0.042 x.max=0.062 y.min=0.011 y.max=0.016
doping uniform n.type conc=1e12 x.min=0.020 x.max=0.031 y.min=0.006 y.max=0.021
doping uniform n.type conc=1e12 x.min=0.031 x.max=0.042 y.min=0.006 y.max=0.021

# Mapping increased dielectric modulation factor representing complete MCF-7 cell filling
material material=cavity user.group=insulator user.default=oxide permittivity=27.5

contact name=gate work=4.1
contact name=gate2 work=4.1 common=gate
contact name=source
contact name=drain

models srh boltzmann fermi cvt bgn bbt.nonlocal qtunn.dir=xdir

method newton trap maxtraps=50
output p.quantum band.temp con.band val.band band.par

solve init
solve vdrain=1.0 name=drain
log outf="MCF7_K27.5.log"
solve vgate=0.0 name=gate vstep=0.1 vfinal=2.0
log off
save outf="MCF7_K27.5.str"

extract init infile="MCF7_K27.5.log"
extract name="vt1_MCF7" (xintercept(maxslope(curve(v."gate",i."drain"))))
extract name="Ion_MCF7" (max(abs(i."drain")))
extract name="Ioff_MCF7" (min(abs(i."drain")))
extract name="Ratio_MCF7" ((max(abs(i."drain")))/(min(abs(i."drain"))))
extract name="gm_MCF7" (slope(maxslope(curve(abs(v."gate"),abs(i."drain")))))


# -------------------------------------------------------------------------
```

```
# MODULE 6: SIMULATION ITERATION FOR HIGH-RISK T47D TUMOR VARIANT (k = 32.0)
# ------------------------------------------------------------------------
go atlas

mesh space.mult=1.0

x.mesh loc=-0.002 spacing=0.001
x.mesh loc=0.000  spacing=0.001
x.mesh loc=0.015  spacing=0.001
x.mesh loc=0.020  spacing=0.00005
x.mesh loc=0.023  spacing=0.00005
x.mesh loc=0.031  spacing=0.0001
x.mesh loc=0.042  spacing=0.00005
x.mesh loc=0.062  spacing=0.001
x.mesh loc=0.064  spacing=0.001

y.mesh loc=-0.002 spacing=0.001
y.mesh loc=0.000  spacing=0.001
y.mesh loc=0.005  spacing=0.0005
y.mesh loc=0.006  spacing=0.0002
y.mesh loc=0.011  spacing=0.0005
y.mesh loc=0.016  spacing=0.001
y.mesh loc=0.021  spacing=0.0005
y.mesh loc=0.027  spacing=0.001
y.mesh loc=0.029  spacing=0.001

qtx.mesh loc=0.015 spac=2.5e-4
qtx.mesh loc=0.020 spac=5.0e-5
qtx.mesh loc=0.023 spac=5.0e-5
qtx.mesh loc=0.031 spac=1.0e-4
qtx.mesh loc=0.042 spac=5.0e-5
qtx.mesh loc=0.047 spac=2.5e-4

qty.mesh loc=0.006 spac=5.0e-4
qty.mesh loc=0.011 spac=2.0e-4
qty.mesh loc=0.013 spac=2.0e-4
qty.mesh loc=0.014 spac=2.0e-4
qty.mesh loc=0.016 spac=5.0e-4
qty.mesh loc=0.021 spac=5.0e-4

region num=1 material=Air       x.min=-0.002 x.max=0.064 y.min=-0.002 y.max=0.029
region num=2 material=Silicon   x.min=0.000  x.max=0.062 y.min=0.006  y.max=0.021
region num=11 material=InAs     x.min=0.020  x.max=0.023 y.min=0.006  y.max=0.021
region num=3 material=Silicon   x.min=0.023  x.max=0.031 y.min=0.006  y.max=0.021
region num=10 material=Silicon  x.min=0.031  x.max=0.042 y.min=0.011  y.max=0.016
region num=4 material=HfO2      x.min=0.031  x.max=0.062 y.min=0.000  y.max=0.011
region num=5 material=SiO2      x.min=0.000  x.max=0.031 y.min=0.005  y.max=0.006
region num=6 material=SiO2      x.min=0.000  x.max=0.031 y.min=0.021  y.max=0.022
region num=7 material=HfO2      x.min=0.031  x.max=0.062 y.min=0.016  y.max=0.027

region num=8 user.material=cavity x.min=0.020 x.max=0.031 y.min=0.000 y.max=0.005
region num=9 user.material=cavity x.min=0.020 x.max=0.031 y.min=0.022 y.max=0.027

electrode name=gate  x.min=0.020 x.max=0.042 y.min=-0.001 y.max=0.000
electrode name=gate2 x.min=0.020 x.max=0.042 y.min=0.027  y.max=0.028
```

```
electrode name=source x.min=-0.002 x.max=0.000 y.min=0.006 y.max=0.021
electrode name=drain  x.min=0.062  x.max=0.064 y.min=0.011 y.max=0.016

doping uniform p.type conc=1e20 x.min=0.000 x.max=0.020 y.min=0.006 y.max=0.021
doping uniform n.type conc=1e18 x.min=0.042 x.max=0.062 y.min=0.011 y.max=0.016
doping uniform n.type conc=1e12 x.min=0.020 x.max=0.031 y.min=0.006 y.max=0.021
doping uniform n.type conc=1e12 x.min=0.031 x.max=0.042 y.min=0.006 y.max=0.021

# Calibrating the peak permittivity constant (k=32) tracking maximum band bending
material material=cavity user.group=insulator user.default=oxide permittivity=32.0

contact name=gate work=4.1
contact name=gate2 work=4.1 common=gate
contact name=source
contact name=drain

models srh boltzmann fermi cvt bgn bbt.nonlocal qtunn.dir=xdir

method newton trap maxtraps=50
output p.quantum band.temp con.band val.band band.par

solve init
solve vdrain=1.0 name=drain
log outf="T47D_K32.log"
solve vgate=0.0 name=gate vstep=0.1 vfinal=2.0
log off
save outf="T47D_K32.str"

# Final parameters log execution matching maximum threshold shift constraints
extract init infile="T47D_K32.log"
extract name="vt1_T47D" (xintercept(maxslope(curve(v."gate",i."drain"))))
extract name="Ion_T47D" (max(abs(i."drain")))
extract name="Ioff_T47D" (min(abs(i."drain")))
extract name="Ratio_T47D" ((max(abs(i."drain")))/(min(abs(i."drain"))))
extract name="gm_T47D" (slope(maxslope(curve(abs(v."gate"),abs(i."drain")))))

quit
```

Shishir Report

by Shishir Report Shishir Report

Submission date: 09-Jun-2026 06:41PM (UTC+0530)

Submission ID: 2979747948

File name: Shishir_Bhargav_thesis_1.pdf (3.24M)

Word count: 11677

Character count: 58603

Chapter 1

INTRODUCTION

1.1 Clinical Background of Breast Cancer and diagnostic challenges

Malignant oncology is still one of the biggest public health problems of the modern era and breast cancer is the leading cause of mortality and incidence of cancer in women worldwide [1]. Demographic assessments and epidemiological reviews indicate a growing trend of diagnosis in all regions of the world, developed and developing, making early detection a critical clinical necessity [2, 3].

Survival rates are heavily dependent on the clinical stage at diagnosis. If the malignant transformation is detected early, while it is still localized to the primary epithelial tissues, the five-year survival rate is over 90%. However, in cases of regional or distant metastasis, treatment options are limited and the survival rates are significantly reduced.

Major operational bottlenecks plague conventional diagnostic pathways despite the critical need for early detection. The standard screening methods are mammography, magnetic resonance imaging (MRI), propagation-based phase-contrast tomography and high-resolution ultrasound networks [6]. These systems provide structural information, but they often have difficulties in detecting micro-calcifications or subtle tumor shapes in the early development stages leading to false-negative results.

Clinical workflows confirm suspicious screening results by tissue biopsies followed by histopathological verification, or serum-based protein biomarker tracking using Enzyme-Linked Immunosorbent Assays (ELISA) [5]. These sophisticated laboratory workflows are highly accurate but depend on complex infrastructure, expensive chemical reagents and significant processing time. Such a delay in reporting may slow down clinical decision making and adversely affect the patient's prognosis.

1.2 Point-of-Care Diagnostics and Label-Free Biosensing Concepts

Clinical research is shifting to decentralized Point-of-Care (POC) diagnostic paradigms to overcome the constraints of centralized laboratory testing. A practical POC system should be small, inexpensive, easy to use without special training, and able to provide fast and reliable readouts directly in resource-limited settings [4]. To achieve these goals, the shift from traditional label-based bio-detection methods to direct label-free electronic detection frameworks is required.

The most common labeled sensing strategies are based on the conjugation of a secondary reporter agent (fluorescent dye, radioactive isotope or active enzyme) to the target analyte to generate a measurable output signal. This labelling is sensitive but complicated by multiple washing steps, precise chemical preparation and expensive optical reading systems.

In contrast, label-free solid-state biosensing networks directly sense biological binding events. Binding of a target molecule or whole cell to the sensor surface leads to an immediate change in the local electrical properties, e.g. interface potential, capacitive coupling or current density. This simple conversion of biological interactions into electronic signals eliminates the need for complex chemical processing, reduces the cost of testing and enables real-time diagnostic platforms that are compatible with mass production.

1.3 Dielectric Modulation Picture and Solid State Interfaces

The coupling of solid-state microelectronic devices with biological media has resulted in the development of field-effect transistor (FET) biosensors. Historically, this architecture has been achieved by modifications of conventional Metal-Oxide-Semiconductor Field-Effect Transistor (MOSFET) topologies [5]. This technique eliminates the conventional metal gate electrode and thus directly exposes the underlying gate dielectric insulation layer to the target environment. The surface-immobilized capture receptors interact with target biomolecules having a net electric charge and alter the distribution of their charges and thus modulating the output drain current by changing the electrostatic potential at the channel interface.

However, charge-based field-effect sensing is severely constrained by physical limitations in high salinity physiological buffers due to ionic screening. Mobile counter-ions present in the solution screen the molecular charge of the target analyte and form an electrical double layer that could obscure the binding signal if it occurs outside the characteristic Debye length.

The dielectric modulation framework has been proposed to overcome this limitation. A physical nanocavity is etched directly in the gate oxide stack, taking advantage of the intrinsic dielectric properties of the biological target, instead of the net charge of a molecule. The introduction of a target biological specimen

into the sensing nanogap replaces the empty air medium ($k = 1.0$), changing the overall gate capacitance and modulating the device electrical characteristics.

1.4 The Subthreshold Swing Constraint and the Boltzmann Tyranny

While dielectric-modulated MOSFET biosensors offer a viable approach for label-free screening, their practical performance is fundamentally limited by a core physical barrier known as the Boltzmann tyranny [9]. In any standard field-effect transistor operating via thermionic carrier injection, electrons must overcome an energy barrier at the source-channel junction through thermal activation. The efficiency of this switching behavior is measured by the subthreshold swing (SS), which reflects the change in gate voltage required to alter the output current by one order of magnitude:

$$SS = \frac{dV_{gs}}{d(\log_{10} I_{ds})} = \ln(10) \cdot \frac{k_B T}{q} \cdot \left(1 + \frac{C_d}{C_{ox}}\right) \tag{1.1}$$

where k_B is the Boltzmann constant, T is the absolute operating temperature, q is the elementary electronic charge, C_d is the depletion layer capacitance, and C_{ox} is the gate oxide capacitance stack. At room temperature ($T = 300$ K), this physical mechanism sets an absolute theoretical lower floor:

$$SS_{\text{limit}} = \ln(10) \cdot \frac{k_B T}{q} \approx 59.6 \text{ mV/decade} \tag{1.2}$$

As C_{ox} drops, the body factor factor $((1 + C_d/C_{ox}))$ increases significantly, often surpassing the practical subthreshold swing of MOSFET biosensors beyond 120 mV/decade [11, 10]. Subthreshold degradation reduces the voltage sensitivity margin of the device, increases the static power leakage (I_{OFF}) and can mask subtle biological signals behind the thermal noise floors, rendering the standard MOSFET configurations impractical for ultra-low power portable screening nodes.

1.5 Steep Slope Core Sensors using Tunnel Field Effect Transistors

Tunnel Field Effect Transistors (TFETs) have been proposed as a promising steep-slope alternative for high-sensitivity solid-state biosensing to overcome the limitations of thermionic injection barrier [12]. A TFET utilizes the quantum mechanical Band-to-Band Tunneling (BTBT) through an asymmetric heavily doped $p^+ - i - n^+$ junction structure [9] which completely alters the carrier injection mechanism.

When the device is off, the huge energy barrier between the valence band edge of the p^+ source and the conduction band edge of the intrinsic channel prevents

carrier transport, resulting in ultra-low leakage. A positive gate bias pulls down the energy bands inside the channel region sharply, leading to a narrow spatial tunneling window at the junction interface. We model the carrier generation rate in this localized tunneling barrier using Kane's expression:

$$G_{\mathrm{BTBT}} = A_{\mathrm{Kane}} \cdot \frac{E^2}{E_g^{1/2}} \cdot \exp\left(-B_{\mathrm{Kane}} \cdot \frac{E_g^{3/2}}{E}\right) \quad (1.3)$$

where E is the localized electric field profile across the junction, E_g is the material energy bandgap, and A_{Kane}, B_{Kane} are material-dependent scaling constants [25].

Since the carrier generation rate depends exponentially on the local electric field (E), changes in the gate capacitance due to dielectric cavity modulation scale the output drive current (I_{ds}) exponentially [14]. This steep current response enables TFET architectures to overcome the Boltzmann limit and achieves subthreshold swing values well below the thermionic floor ($SS < 60$ mV/dec) at room temperature, providing exceptional sensitivity to subtle changes in cavity permittivity [13, 7].

1.6 Structural innovations in pocket engineering and heterojunction

Silicon-based homojunction TFET devices exhibit excellent subthreshold swing properties. They however often suffer from low on-state drive currents (I_{ON}) due to the relatively large effective mass of electrons in bulk silicon and its wide indirect bandgap. To overcome this drive current bottleneck, and to maximize the sensitivity margins, two major structural innovations are incorporated in modern TFET architectures: pocket engineering and heterojunction material design [19, 22].

Pocket engineering: introduction of an ultra-thin, highly doped semiconductor region at the source-channel interface. This localized dopant density significantly enhances the electric field gradient in the junction, reducing the depletion width and greatly enhancing the tunnelling probability. This pocket can be implemented with other low bandgap materials such as Indium Arsenide (InAs) to have heterojunction interface for further improvement of transport kinetics.

The small bandgap of InAs lowers the height of the potential barrier for carriers to cross, greatly enhancing the rate of band-to-band tunneling. This pocket-engineered heterojunction configuration, along with a dielectrically modulated gate nanocavity, ensures that small variations in target cell permittivity result in large and readily detectable variations in output current, providing an excellent framework for high-sensitivity whole-cell screening platforms [8].

1.7 Structure of the Thesis Document

The research and engineering characterization work presented in this dissertation report is organized systematically into five main chapters:

- **Chapter 1: Introduction** gives a brief overview of early clinical paradigms of breast cancer diagnostics, the requirements of point-of-care testing, the basics of label-free solid-state sensing, limitations of field-effect device physics and the key structural objectives of this project.
- **Chapter 2: Literature Review and Problem Identification:** A survey on previous engineering trends, various device topologies, charge plasma modeling rules, a detailed analysis of recent literature benchmarks, and a formal statement of the research gaps and project objectives.
- **Chapter 3: Device Architecture and TCAD Simulation Methodology** discusses the exact architectural coordinate layout, material compositions, asymmetric high-k/low-k gate stack optimizations, and physical simulation models calibrated in the Silvaco ATLAS TCAD environment along with a feasible CMOS-compatible process integration flow.
- **Chapter 4: Results and Discussion** contains the full set of numeric observation data including linear and logarithmic transfer responses, surface electrostatic potential profiles, junction electric field distributions, transconductance curves, selectivity ratios, voltage sensitivity metrics, and a full analysis of partial cavity occupancy variations.
- **Chapter 5: Conclusion, Future Scope and Social Impact** summarizes the main research outcomes, evaluates the immediate clinical and social impact of decentralized screening platforms and discusses future technological research directions for multi-target microfluidic on-chip integration.

Chapter 2

REVIEW OF LITERATURE AND PROBLEM IDENTIFICATION

2.1 Subthreshold and the thermionic limit Bottleneck Swing

Solid state field-effect architectures are commonly employed in modern point-of-care diagnostics. Traditionally, conventional MOSFET topologies have been modified for label free biological sensing by directly exposing the gate dielectric layer to biological targets [5]. In these classical designs, the injection of carriers from the source to the channel is controlled by thermionic emission over a controllable potential barrier.

Mathematically, the electrostatic switching performance of any thermionic transistor is bounded by its subthreshold swing (SS):

$$SS = \frac{dV_{gs}}{d(\log_{10} I_{ds})} = \ln(10) \cdot \frac{k_B T}{q} \cdot \left(1 + \frac{C_d}{C_{ox}}\right) \tag{2.1}$$

where k_B is the Boltzmann constant, T is the operating temperature, q is the electronic charge, C_d is the depletion layer capacitance and C_{ox} is the gate oxide capacitance. This transport mechanism imposes an absolute physical lower bound at ambient temperature ($T = 300$ K):

$$SS_{\text{limit}} = \ln(10) \cdot \frac{k_B T}{q} \approx 59.6 \text{ mV/decade} \tag{2.2}$$

called the Boltzmann thermal limit [9]. The insertion of a physical sensor nanocavity in a typical MOSFET gate stack results in a dramatic decrease of the effective gate capacitance due to the serial insertion of an air gap ($k = 1$). This reduction in C_{ox}, according to Eq. 2.1, leads to a significant degradation of the subthreshold swing, often pushing practical MOSFET biosensors to $SS \geq 120$ mV/decade [11], which reduces voltage sensitivity and results in high standby power leakage.

2.2 Physics of dielectric modulation for label-free detection

Dielectric modulation avoids chemical labels by treating the sensing nanogap as an open dielectric waveguide. When target biological cells are trapped inside the cavity space, they displace the baseline air medium ($k = 1.0$) and change the overall capacitance profile of the gate stack.

The effective capacitance of the dual layer sensing gate insulator is given by:

$$C_{\text{eff}} = \frac{C_{\text{ox}} \cdot C_{\text{cav}}}{C_{\text{ox}} + C_{\text{cav}}} = \frac{\epsilon_0 \cdot \epsilon_{\text{ox}} \cdot \epsilon_{\text{bio}}}{\epsilon_{\text{bio}} \cdot T_{\text{ox}} + \epsilon_{\text{ox}} \cdot T_{\text{cav}}} \tag{2.3}$$

where ϵ_0 is the vacuum permittivity, ϵ_{ox} and ϵ_{bio} are the relative permittivities of the oxide and the target biomolecule, respectively, T_{ox} is the remaining oxide thickness and T_{cav} is the physical thickness of the carved cavity space.

High-κ species bind in the cavity, leading to an instantaneous increase of C_{eff} as ϵ_{bio} moves upwards. This capacitive boost down-shifts the threshold voltage and alters the vertical electric field profile inside the underlying semiconductor channel layer without any external change in the net molecular charge. Precise change of current output and transconductance are mapped for the screening of targets.

2.3 Steep Slope Core Sensors: Tunnel Field-Effect Transistors

The thermionic injection limitation is completely overcome by the Tunnel Field-Effect Transistors (TFET) utilizing quantum mechanical Band-to-Band Tunneling (BTBT) through a designed asymmetric junction [10]. A TFET is a gated $p^+ - i - n^+$ diode design with reverse bias. When a positive gate bias (V_{gs}) is applied, the energy bands are pulled down sharply in the intrinsic channel region, allowing electrons to tunnel directly from the source valence band to the channel conduction band.

The quantum rate of generation of carriers across this confined tunneling barrier takes the non-local analytical expressions of Kane:

$$G_{\text{BTBT}} = A_{\text{Kane}} \cdot \frac{E^2}{E_g^{1/2}} \cdot \exp\left(-B_{\text{Kane}} \cdot \frac{E_g^{3/2}}{E}\right) \tag{2.4}$$

where E is the localized electric field profile across the junction, E_g is the target semiconductor material energy bandgap, and A_{Kane}, B_{Kane} are material-dependent scaling constants [25]. The generation rate scales exponentially with junction electric field (E).

Modulation of the dielectric cavity induces fluctuations in the gate capacitance resulting in exponential scaling of the output drive current (I_{ds}). This steep current response enables TFETs to achieve subthreshold swing values well below

the 60 mV/dec thermionic limit ($SS < 60$ mV/dec) at room temperature, causing them to be very sensitive to small electrostatic variations [12].

2.4 Literature Trends: Engineering Critical Analysis

The architectural development from planar silicon devices to complex multi-gate heterojunction architectures has been widely studied in the field of solid-state biosensing. The initial implementation frameworks confirmed that the combination of the TFET devices with a carved dielectric gap allowed variations in cavity permittivity to produce major changes in output tunneling current leading to significantly higher electrical sensitivity margins compared to traditional MOSFET alternatives [14].

For these baseline models there are different design guidelines for different configurations to improve. The investigation of dielectrically modulated dopingless TFET structures has been explored through charge plasma techniques with specified metal work functions to realize virtual source and drain extensions [29]. This approach is effective in mitigating the high thermal budgets and the random dopant fluctuation (RDF) problems of conventional junctions, although the baseline drive currents are limited by the carrier mass in silicon.

Topologies with localized source-side pockets are also investigated to mitigate the drive current bottleneck [30]. One must be careful to consider the constraints due to steric hindrance in the related nanogaps. The introduction of highly doped pocket areas at the tunneling junction reduces the width of the depletion layer, which in turn greatly enhances the carrier injection rates. Simultaneously, the integration of two-dimensional material channels is reported, based on Si-doped MoS_2 thickness-engineered layouts optimized for breast cancer cell screening applications [8]. The study proved that malignant cell lines have higher relative permittivity properties than healthy tissues as a result of variation of intracellular water content and changed protein structures.

More recently, performance enhancement was focused on the incorporation of alternative low bandgap chemicals within pocket-engineered heterojunction frameworks [19, 22]. Adding a thin, epitaxially grown layer of InAs at the source–channel interface forms a pocket and reduces the effective tunneling barrier height, giving much higher overall drive currents. Moreover, it has been reported that the employment of dual symmetric nanocavity arrays can produce robust multi-line whole-cell screening profiles that allow successful classification of different tumor grades from distinct capacitive shifts [20].

2.5 Identification of the Central Research Gap

Despite the above structural and material breakthroughs in the field effect biosensing, a critical appraisal of the current engineering landscape reveals some unresolved challenges:

1. **The On-Current vs. Ambipolarity Tradeoff:** Pocket-engineered homojunction TFETs improve on-state drive currents, but heavy doping in these narrow regions leads to strong ambipolar conduction in negative gate-to-drain bias. This increases static power leakage and decreases the clean sensing window.

2. **Subthreshold Degradation for Low Permittivity Loadings:** The majority of the existing dielectric-modulated TFET biosensors demonstrate a degradation in capacitive coupling when a large portion of the gate stack is transformed into a physical cavity. In tracking lower-permittivity species, the subthreshold swing deteriorates well beyond 100 mV/dec, masking tiny biological signals behind high thermal noise floors.

3. **No Strong Whole-Cell Multi-Line Discriminability with Partial Filling Constraints:** Most models are based on an idealized scenario where biomolecules homogeneously occupy 100% of the nanocavity. In real sample delivery, the filling is usually not complete, the orientation is unpredictable, and there is steric hindrance inside the nanogap. No comprehensive multi-line classification profiles mapping the electrical response of specific breast cancer cell line variants—healthy reference cells (**MCF-10A**, $k = 4.5$) versus malignant lines (**Hs578T**, $k = 22.0$; **MDA-MB-231**, $k = 24.5$; **MCF-7**, $k = 27.5$; and **T47D**, $k = 32.0$)—across varying filling intervals exist.

2.6 Scope and Objectives of the Present Dissertation

This research tackles these limitations by designing, optimizing and evaluating a new Pocket-Engineered Dielectric-Modulated Heterojunction TFET Biosensor tailored for label-free breast cancer cell classification. The explicit objectives of this research work are categorized under three main implementation phases:

- **Junction and Energy-Band Engineering:** Introduce a thin 3 nm InAs pocket layer at the source-channel interface to reduce the effective tunneling barrier height and maximize driving current. This, together with an asymmetric hetero-dielectric gate stack (SiO_2 on the source side for minimizing parasitic capacitance and HfO_2 on the drain side for enhanced electrostatic control) suppresses the ambipolar leakage.

- **Strictly Calibrated TCAD Simulation Platform:** Build and run a complete physics-based numeric simulation matrix using the Silvaco ATLAS environment. This paradigm links non-local quantum band-to-band tunneling dynamics with Lombardi CVT mobility degradation and Shockley-Read-Hall trapping to capture realistic device physics under low-power operating profiles.

- **Whole-Cell Selectivity and Occupancy Robustness Profiling:** Evaluate the electrical response of the device against well-characterized breast cancer cell lines and plot the specified metrics (V_{th}, I_{ds}, g_m, and SS) as a function of permittivity. Finally, monitor performance at discrete cavity filling levels (25%, 50%, 75%, and 100%) to confirm that the sensor generates distinct, noise-immune diagnostic signatures even with partial target loading.

Chapter 3

DEVICE ARCHITECTURE AND TCAD SIMULATION METHODOLOGY

3.1 Device Architecture

The suggested biosensor is based on a TFET architecture integrating a hetero-junction pocket to boost tunneling efficiency. Fig. 3.1 displays the schematic perspective of the proposed TFET biosensor, indicated with crucial geometrical parameters.

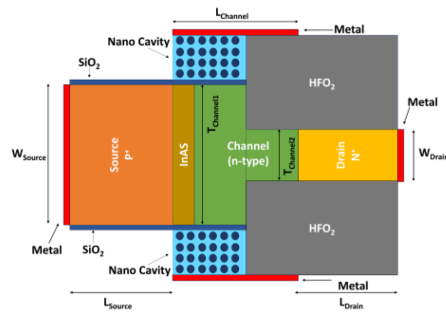

Figure 3.1: Cross-sectional schematic of the proposed pocket-engineered TFET biosensor with annotated device dimensions conforming to Table 3.1.

The particular geometrical dimensions and doping concentrations employed in this simulation are reported in Table 3.1. The device has a channel architecture which provides for aggressive footprint scaling while preserving adequate channel management.

The gate stack features a novel hetero-dielectric configuration to optimize device performance. To improve stability and reduce parasitic capacitance at the

Table 3.1: Design Parameters of the Proposed TFET Biosensor

Parameter	**Symbol**	**Value**
Channel Length	L_{channel}	22 nm
Source/Drain Pocket Length	L_{pocket}	3 nm
Nanocavity Length	L_{cav}	11 nm
Nanocavity Width	T_{cav}	5 nm
Gate Oxide Thickness	T_{ox}	1 nm
Thickness of Sensing Cavity	T_{channel1}	15 nm
Control Channel Thickness	T_{channel2}	5 nm
Source Doping (P^+)	N_S	1×10^{20} cm^{-3}
Drain Doping (N^+)	N_D	1×10^{18} cm^{-3}
Channel Doping (N^-)	N_{ch}	1×10^{12} cm^{-3}
Pocket Material	-	InAs
Source Dielectric (Thicker Side)	-	SiO_2
Drain Dielectric (Thinner Side)	-	HfO_2
Gate Work Function	Φ_M	4.1 eV

tunneling junction, a Low-κ dielectric (SiO_2) is used on the source side of the thicker channel (T_{channel1}). On the other hand, the electrostatic control at the drain side, where the channel is narrower (T_{channel2}), is increased by using a High-κ dielectric (HfO_2) [23, 24].

3.2 Simulation Models

The device simulations were performed using the Silvaco ATLAS TCAD tool. To properly forecast the electrical characteristics and biosensing performance, appropriate physical models were calibrated based on known semiconductor physics.

First and foremost, Kane's Band-to-Band Tunneling (BTBT) model is utilized. Since TFETs work by quantum mechanical tunneling rather than thermal emission, standard drift-diffusion models are inadequate. Kane's model calculates the carrier production rate at the source-channel tunneling junction based on the local electric field and the bandgap of the material [25].

To account for trap-assisted recombination, which is crucial for simulating leakage currents in the subthreshold regime (the "off" state), the Shockley-Read-Hall (SRH) recombination model is incorporated [17]. This guarantees realistic and non-artificially low simulated off-currents (I_{OFF}).

Additionally, the Lombardi CVT model is applied to simulate mobility decline. This complete mobility model accounts for degradation owing to transverse acoustic phonon scattering, surface roughness scattering at the oxide interface, and scattering produced by vertical electric fields. This is crucial for biosensors

as the surface contact quality can dramatically effect sensitivity [26]. Finally, Fermi-Dirac statistics are activated to adequately describe carrier distribution in the highly doped source (10^{20} cm^{-3}) and drain regions, where the simpler Boltzmann approximation becomes inappropriate.

3.3 Fabrication Process Flow

The suggested fabrication process flow is given in Fig. 3.2 and employs a conventional CMOS-compatible flow, assuring the device may be produced employing current foundry capabilities.

A Silicon-On-Insulator (SOI) wafer is used to start the process **(a)**. In order to reduce parasitic leakage currents from the substrate and obtain superior electrical isolation, SOI technology is used. Next, asymmetric ion implantation is done to define the highly doped P-type Source and N-type Drain regions **(b)**, followed by rapid thermal annealing (RTA) for dopant activation.

A thin 3 nm InAs pocket layer is epitaxially grown at the source junction **(c)**. Indium Arsenide (InAs) has a shorter bandgap than Silicon, which considerably lowers the tunneling barrier width and enhances the on-current (I_{ON}) [27]. Step **(d)** involves creating a dual-thickness channel profile by a Reactive Ion Etch (RIE), which defines the sensing and control regions.

A High-κ dielectric layer (HfO_2) is then created using Atomic Layer Deposition (ALD) **(e)**. ALD is needed here to ensure conformal coverage of the sidewalls and a high-quality interface with minimum flaws [28]. The oxide is then shaped and etched **(f)** to reveal the sensing area where biomolecules will be attached.

To create the sensing void, a sacrificial layer (usually polysilicon or oxide) is placed **(g)** and etched back to form the nanocavity **(h)** near the source junction [14]. The metal gate electrode is placed using sputtering **(h)** over the control oxide. Isolation is obtained by etching the substrate from the backside using the Buried Oxide (BOX) layer as an etch-stop **(i)**. Finally, wafer bonding techniques for structural integration and contact metallization are completed **(j)** to construct the device terminals suitable for testing.

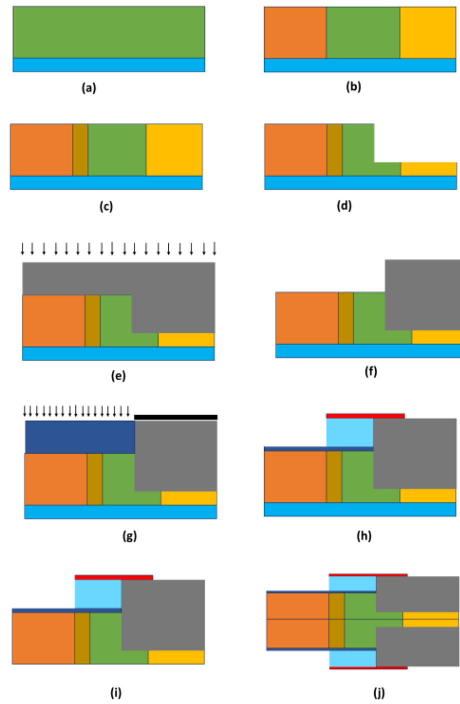

Figure 3.2: Proposed fabrication process flow for the TFET biosensor: (a) SOI Substrate Preparation; (b) Ion Implantation for Source/Drain; (c) Epitaxial Growth of InAs Pocket; (d) Channel Etching to define dual-thickness; (e) High-κ Dielectric Deposition; (f) Oxide Patterning; (g) Sacrificial material and Low-κ Deposition; (h) Sacrificial Etch for Nanocavity and Metal Gate Deposition; (i) Backside Etching; (j) Finalization, wafer bonding, and Contact Metallization.

Chapter 4

RESULTS AND DISCUSSION

The electrical characteristics of the suggested pocket-engineered DM-TFET are mainly determined by the dielectric properties of the biological materials within the nanocavity. Table 4.1 summarizes the specific breast cancer cell lines and the healthy reference cell used in this simulation, along with their respective dielectric constants (k).

Table 4.1: Various Cell Lines with Corresponding Dielectric Constants (k)

Cell Line	Dielectric Constant (k)	Nature	Ref.
MCF-10A	4.5	Healthy Breast Cell	[8]
Hs578T	22.0	Cancer Cell	[8]
MDA-MB-231	24.5	Cancer Cell	[8]
MCF-7	27.5	Cancer Cell	[8]
T47D	32.0	Cancer Cell	[8]

4.1 DC Characteristics

The drain current monotonically increases with the dielectric constant of the immobilized cell. The air filled cavity exhibits the lowest current while the T47D cell exhibits the highest current owing to the strongest gate coupling, in agreement with literature [14].

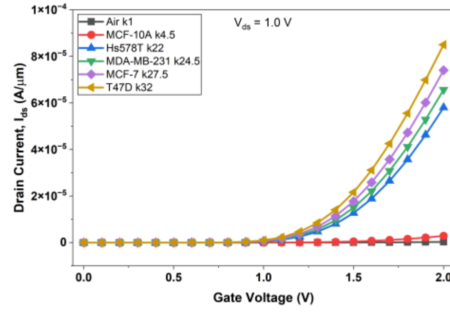

Figure 4.1: Drain current versus gate voltage linear plot I_{ds} vs. V_{gs}.

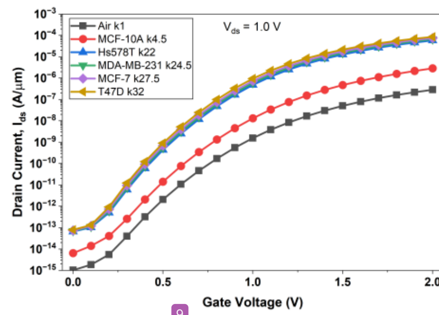

Figure 4.2: Logarithmic plot of Drain Current (I_{ds}) versus Gate Voltage (V_{gs}).

4.2 Surface Potential and Electric Field Analysis

Detection mechanism is electrostatic modulation. The surface potential along the channel is shown in Fig. 4.3. The potential curve is larger and steeper in the case of high dielectric malignant cells (T47D, $k = 32$) indicating more band bending compared to healthy cells.

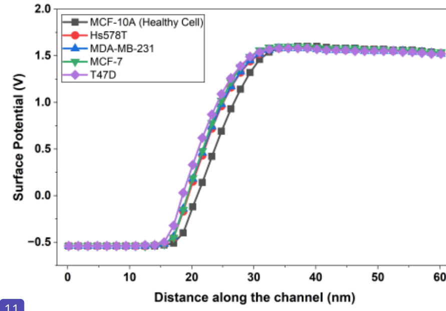

Figure 4.3: Surface potential variation along the channel length for different cell lines.

This gradient has an effect on the electric field (Fig. 4.4). The maximum electric field increases considerably for T47D cells to over 2.3×10^6 V/μm, favoring the tunneling rate through the BTBT mechanism [12].

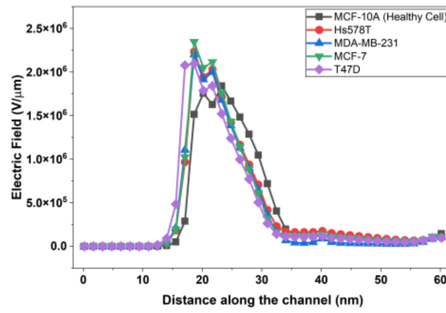

Figure 4.4: Distribution of electric field across the channel length.

4.3 Static & Dynamic Parameter Analysis

To measure the performance, we took static parameters (V_{th}, I_{ON}) and dynamic parameters (g_m, SS). Fig. 4.5 shows the Threshold Voltage (V_{th}) and On-Current (I_{ON}) as a function of cell type. The V_{th} is in a decreasing trend from 1.60 V (Healthy) to 1.44 V (T47D) while the I_{ON} increases, which means that the device is activated earlier and shows improved conductivity for malignant cells.

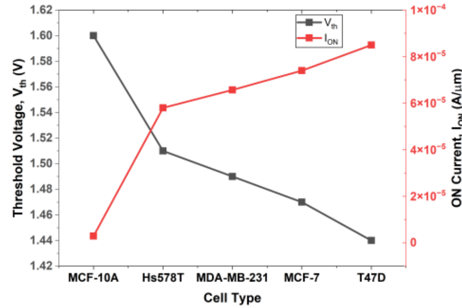

Figure 4.5: Threshold voltage (V_{th}) and on-state current (I_{ON}) variation with cell type.

Figure depicts transconductance (g_m) vs gate voltage for each cell line. 4.6. Compared to healthy cells, malignant cells show a rapid increase of g_m, with higher signal amplification capabilities [29].

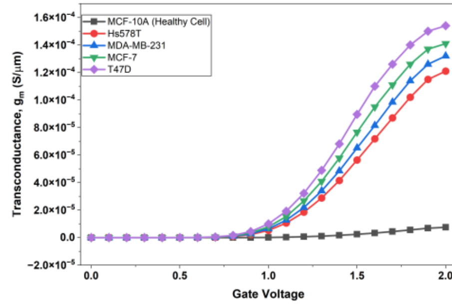

Figure 4.6: Gm (transconductance) vs. V_{gs} (gate voltage) for all the cell lines.

The peak g_m and Subthreshold Swing (SS) are shown in Fig. 4.7. The measured SS is 94.3 mV/dec for high-risk cells. While perfect TFETs can reach

sub-60 mV/dec, the integration of the sensing nanocavity naturally reduces gate coupling, resulting in a slightly larger SS. However, this value remains significantly superior to traditional MOSFET-based biosensors which typically exhibit $SS > 120$ mV/dec, guaranteeing that the proposed device maintains high sensitivity and distinct switching.

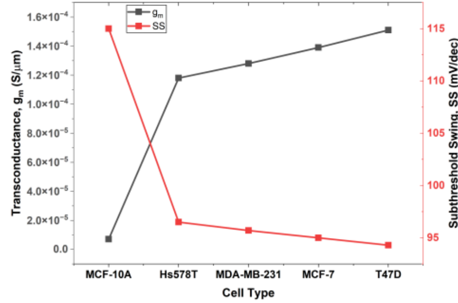

Figure 4.7: Peak Transconductance (g_m) and Subthreshold Swing (SS) obtained for each cell type.

4.4 Selectivity Analysis

Selectivity (S) is defined as the ratio of the drain current of the target cell to that of the healthy reference cell. As illustrated in Fig. 4.8, the proposed pocket-engineered DM-TFET demonstrates a remarkable selectivity profile. For the high-risk T47D cell line ($k = 32$) the device obtains a selectivity factor of 29.6. This means that the current signal generated by the cancer cells is roughly 30 times stronger than that of healthy cells. This significant margin is related to the nonlinear dependency of the tunneling probability on the gate capacitance. The high dielectric constant of malignant cells significantly raises the electric field at the source junction, dramatically enhancing the tunneling generation rate compared to the low-dielectric healthy cells. Such strong selectivity is crucial for early-stage diagnosis, because the concentration of malignant cells may be low relative to the background of healthy cells, providing a low false-positive rate and high diagnostic confidence.

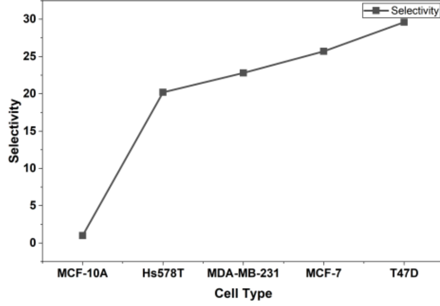

Figure 4.8: Selectivity of the biosensor normalized to the healthy MCF-10A cell.

4.5 Sensitivity Analysis

The sensitivity of the proposed biosensor for cancer detection is determined using the standard expression:

$$S(x) = \frac{x_{bio} - x_{air}}{x_{air}} \tag{4.1}$$

Where x is the computed sensitivity electrical parameter (such as I_{ds}, V_{th}, or g_m), x_{bio} is the electrical parameter measured when the cavity is filled with the specific cancer cell line, and x_{air} is the electrical parameter when the cavity is empty.

4.5.1 Threshold Voltage Sensitivity (ΔV_{th})

The absolute change in threshold voltage with respect to the air-filled cavity is known as the threshold voltage sensitivity:

$$\Delta V_{th} = V_{th(air)} - V_{th(bio)} \tag{4.2}$$

where $V_{th(air)}$ is the threshold voltage when there is air in the cavity and $V_{th(bio)}$ is the threshold voltage when there is a biomolecule present. As the dielectric constant increases, sensitivity steadily increases, as seen in Fig. 4.9. For example, the shift is small in healthy MCF-10A cells ($k = 4.5$). For high-risk T47D cells ($k = 32$), the device's maximal sensitivity is 130 mV. This significant shift is useful for real-world sensing applications as it produces a distinct, quantifiable signal that is resistant to noise and exceeds the sensitivity levels seen in similar doping-less TFET devices [29].

4.5.2 Sensitivities of Drain Currents (SIDs)

The drain current sensitivity is calculated using $x = I_{\text{ds}}$ in Eq. 4.1. Fig. 4.10 shows S_{Ids} reaching a maximum of 606 for T47D cells at $V_{\text{gs}} = 1.0$ V. The explicit

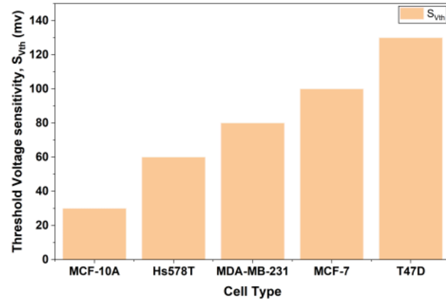

Figure 4.9: Fig. 4.9. Sensitivity of the Threshold Voltage (ΔV_{th}) with respect to Air.

computation is:

$$S_{Ids} = \frac{I_{ds(bio)} - I_{ds(air)}}{I_{ds(air)}} \tag{4.3}$$

Fig. 4.11 shows strong sensitivity ($S_{\text{Ion}} \approx 297$) even for high gate voltages ($V_{\text{gs}} = 2.0$ V), which indicates the substantial slope advantage of the TFET [8].

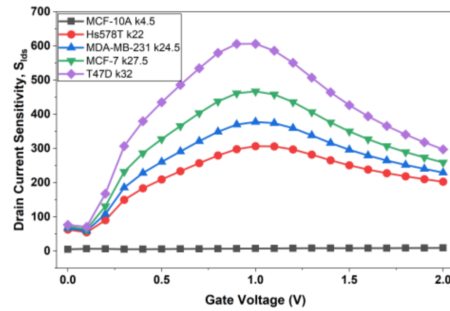

Figure 4.10: Drain Current Sensitivity (S_{Ids}) versus Gate Voltage.

Furthermore, a huge dynamic sensitivity (S_{gm}) of 228 is seen in Fig. 4.12. Transconductance sensitivity is a critical figure of merit for analog sensing applications as it measures the shift in the device's capability for amplification after the immobilization of biomolecules. This high result demonstrates that the presence of T47D cancer cells ($k = 32$) not only shifts the threshold voltage but also greatly enhances the gate control efficiency across the channel. Consequently, even minute changes in the biomolecule concentration may be detected as large variances in

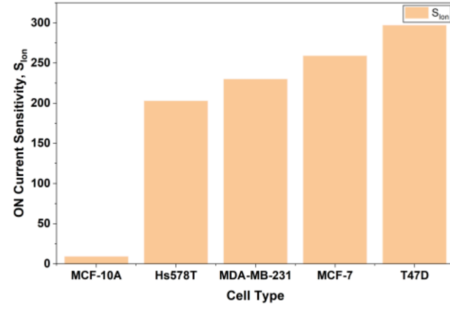

Figure 4.11: ON-Current Sensitivity (S_{Ion}) at $V_{gs} = 2.0$ V.

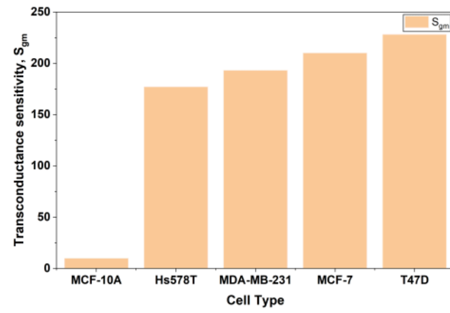

Figure 4.12: Transconductance Sensitivity (S_{gm}) relative to Air.

the device's switching speed, affording a unique advantage over standard sensors that depend only on static current shifts.

4.6 Impact of Biomolecule Occupancy

Because of steric barrier, surface roughness, or the random orientation of biomolecules during the immobilization process, it could be problematic to guarantee 100% filling of the nanocavity in real-world biological sensing conditions. Therefore, studying the sensor's responsiveness under partial filling situations is crucial for assessing its resilience and reliability in real-world applications. We simulated the nanocavity's fill factor for both malignant (T47D) and healthy (MCF-10A) cell lines at different intervals, such as 25%, 50%, 75%, and 100%.

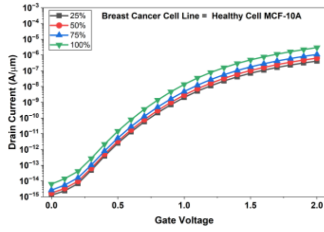

Figure 4.13: Impact of occupancy on transfer characteristics for healthy MCF-10A cells.

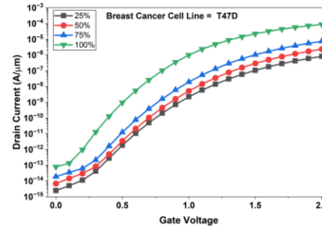

Figure 4.14: Impact of occupancy on transfer characteristics for high-risk T47D cells.

The transfer characteristics for healthy MCF-10A cells are shown in Fig. 4.13. As the occupancy increases, the drain current displays a marginal amplification, about 7 times at full occupancy. This very tiny gain is owing to the lower dielectric constant ($k = 4.5$) of the healthy cells, which offers only a limited improvement in gate coupling.

Fig. 4.14, on the other hand, shows the effect of occupancy for the high-risk T47D cancer cells ($k = 32$). Here the drain current exhibits a huge surge, increasing by almost two orders of magnitude (> 100-times) as the cavity fills. The high dielectric constant of the malignant cells considerably increases the gate oxide capacitance (C_{ox}) which drastically narrows the tunneling barrier width at the source-channel interface. This non-linear, exponential increase of the tunneling probability with occupancy indicates that the sensor is very sensitive to the volume of malignant biological material present. The sensor shows a clear and distinct change in signal at 40–60 % occupancy, which means that detection of high risk cancer cells will not be affected by partial filling.

Fig. 4.15 shows the static parameter shifts. As the increase of the occupancy, the threshold voltage (V_{th}) for cancer cells reduces quickly from 1.62 V to 1.44 V, which indicates the switching properties change a lot. On the other hand, healthy

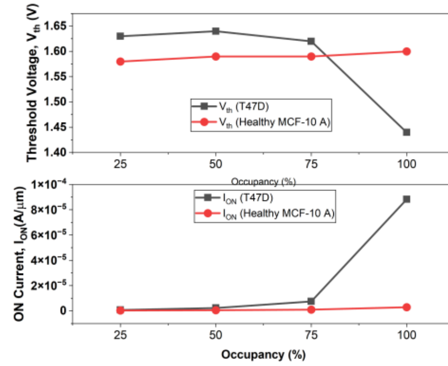

Figure 4.15: Vth and I_{ION} versus occupancy for MCF-10A vs. T47D.

cells have a rather stable V_{th}, which means only a small change. The diagnostic accuracy and the chances of false positives are minimized by the unique electrical responses of healthy and malignant cells even at different occupancy levels.

4.7 Performance Evaluation

The performance of the proposed device is compared with the previously reported TFET based biosensors as shown in Table 4.2. As can be seen from the table, this work has a current sensitivity (S_{Ion}) of 2.97×10^2 and threshold voltage shift (ΔV_{th}) of 130 mV. These values are higher than those reported for the other devices in the comparison.

Table 4.2: Benchmark Comparison: TFET Biosensor Sensitivity

Biosensors	S_{ion}	ΔV_{th} **(mV)**
Ref. [8]	1.1×10^2	–
Ref. [29] (I)	1×10^1	66
Ref. [29] (II)	4×10^1	54
Ref. [30]	2.5×10^2	–
This Work	$\mathbf{2.97 \times 10^2}$	**130**

Chapter 5

CONCLUSION, FUTURE SCOPE AND SOCIAL IMPACT

5.1 Summary of Key Research Findings

This study describes the design and simulation of a pocket-engineered DM-TFET for label-free breast cancer detection. The device exhibits sharper switching behavior than conventional MOSFET-based biosensors. This improvement is achieved by adding a nanocavity at the source-channel tunneling junction and using a hetero-material InAs pocket. The sensor is highly sensitive to changes in the dielectric permittivity of the immobilized cells.

Simulation results show that the device responds strongly to high-risk T47D cells, with a peak transconductance sensitivity of 228 and a peak drain current sensitivity of 606. The results also show that the sensor continues to perform well even when the biomolecule occupancy is partial rather than full. Another clear observation is that cancerous cells produce current spikes almost 100 times higher than those from healthy cells.

5.2 Future Scope and Social Impact

The clinical and social implications of this work are broad. By moving early cancer diagnostics away from invasive infrastructure and tracking shifts dynamically inside an electronic POC node, cost-barriers drop dramatically. Future engineering directives may analyze dynamic microfluidic integration alongside multi-target tracking cells to track multiple structural biomarkers simultaneously.

REFERENCES

[1] F. Bray, J. Ferlay, I. Soerjomataram, R. L. Siegel, L. A. Torre, A. Jemal, Global cancer statistics 2018: GLOBOCAN estimates of incidence and mortality worldwide for 36 cancers in 185 countries, CA: A Cancer J. Clin. 68 (2018) 394–424. https://doi.org/10.3322/caac.21492.

[2] R. L. Siegel, K. D. Miller, A. Jemal, Cancer statistics, 2018, CA: A Cancer J. Clin. 68 (2018) 7–30. https://doi.org/10.3322/caac.21442.

[3] World Health Organization, Breast cancer, Geneva, Switzerland, 2022. [Online]. Available: https://www.who.int/news-room/fact-sheets/detail/breast-cancer

[4] D. N. Elsheakh, O. M. Fahmy, M. Farouk, K. Ezzat, A. R. Eldamak, An early breast cancer detection by using wearable flexible sensors and artificial intelligent, IEEE Access 12 (2024) 48511–48529. https://doi.org/10.1109/ACCESS.2024.3380453.

[5] S. P. Mohanty, E. Kougianos, Biosensors: A Tutorial Review, IEEE Potentials 25 (2006) 35–40. https://doi.org/10.1109/MP.2006.1649009.

[6] A. Aminzadeh, et al., Imaging breast microcalcifications using dark-field signal in propagation-based phase-contrast tomography, IEEE Trans. Med. Imag. 41 (2022) 2980–2990. https://doi.org/10.1109/TMI.2022.3175924.

[7] P. Harika, G. S. Kondavitee, S. R. Karumuri, A. Lay-Ekuakille, High sensitivity of dielectrically modulated tunnel field effect transistor for biosensor applications, IEEE Trans. Nanobiosci. (2024). https://doi.org/10.1109/TNB.2024.3386586.

[8] P. Kaushal, G. Khanna, Breast Cancer Detection Using Si-Doped MoS2 Channel-Based Thickness Engineered TFET Biosensor, IEEE Sensors Lett. 8 (2024) 1–4. https://doi.org/10.1109/LSENS.2024.3438872.

[9] A. M. Ionescu, H. Riel, Tunnel field-effect transistors as energy-efficient electronic switches, Nature 479 (2011) 329–337. https://doi.org/10.1038/nature10679.

[10] J. Appenzeller, et al., Band-to-band tunneling in carbon nanotube field-effect transistors, Phys. Rev. Lett. 93 (2004) 196805. https://doi.org/10.1103/PhysRevLett.93.196805.

[11] T. Krishnamohan, et al., Double-Gate Strained-Ge Heterostructure Tunneling FET (TFET) With record high drive currents and $\leq$ 60mV/dec subthreshold slope, IEEE IEDM (2008). https://doi.org/10.1109/IEDM.2008.4796839.

[12] W. Y. Choi, et al., Tunneling Field-Effect Transistors (TFETs) with Subthreshold Swing (SS) Less Than 60 mV/dec, IEEE Electron Device Lett. 28 (2007) 743–745. https://doi.org/10.1109/LED.2007.901273.

[13] V. Thakur, A. Kumar, S. Kale, Analytical modeling of space engineered reconfigurable silicon nanowire Schottky barrier transistor for biosensing applications, Micro Nanostruct. 188 (2024) 207799. https://doi.org/10.1016/j.micrna.2024.207799.

[14] D. Sarkar, K. Banerjee, Proposal for a Tunnel-Field-Effect-Transistor-Based Dielectric-Modulated Biosensor, Appl. Phys. Lett. 100 (2012) 143108. https://doi.org/10.1063/1.3698093.

[15] C. Li, F. Liu, R. Han, Y. Zhuang, A vertically stacked nanosheet gate-all around FET for biosensing application, IEEE Access 9 (2021) 63602–63610. https://doi.org/10.1109/ACCESS.2021.3074906.

[16] K. Boucart, A. M. Ionescu, Double-Gate Tunnel FET With High-kappa Gate Dielectric, IEEE Trans. Electron Devices 54 (2007) 1725–1733. https://doi.org/10.1109/TED.2007.899389.

[17] S. M. Sze, K. K. Ng, Physics of Semiconductor Devices, 3rd ed., Wiley, 2006. https://doi.org/10.1002/0470068329.

[18] R. Vishnoi, M. J. Kumar, Compact Analytical Model of Dual Material Gate Tunneling Field-Effect Transistor Using Interband Tunneling and Channel Transport, IEEE Trans. Electron Devices 61 (2014) 1936–1942. https://doi.org/10.1109/TED.2014.2315294.

[19] S. R. Upadhyay, S. Kale, A. Pandey, Dielectric Modulated InAs Pocket Heterojunction tunnel FET for biosensor applications, ECS J. Solid State Sci. Technol. 14 (2025) 047006. https://doi.org/10.1149/2162-8777/adc338.

[20] K. N. Priyadarshani, S. Singh, Ultra sensitive breast cancer cell lines detection using dual nanocavities engraved junctionless FET, IEEE Trans. Nanobiosci. 22 (2023) 889–896. https://doi.org/10.1109/TNB.2023.3246106.

[21] R. Pethig, Dielectric and Electrical Properties of Biological Materials, J. Bioelectricity 4 (2009) vii–ix. https://doi.org/10.3109/15368378509033258.

[22] D. Barwa, D. Khanna, H. Parihar, S. Kale, A Novel n+ Pocket Doped L-Shaped Channel TFET for Biosensing Applications, ECS J. Solid State Sci. Technol. 14 (2025) 047010. https://doi.org/10.1149/2162-8777/adccf8.

[23] G. D. Wilk, et al., High-k gate dielectrics: Current status and materials properties considerations, J. Appl. Phys. 89 (2001) 5243–5275. https://doi.org/10.1063/1.1361065.

[24] M. Rahimian, M. Fathipour, Improvement of electrical performance in junctionless nanowire TFET using hetero-gate-dielectric, J. Mater. Sci. Semicond. Process. 63 (2017) 142–152. https://doi.org/10.1016/j.mssp.2016.12.011.

[25] A. C. Seabaugh, Q. Zhang, Low-Voltage Tunnel Transistors for Beyond CMOS Logic, Proc. IEEE 98 (2010) 2095–2110. https://doi.org/10.1109/JPROC.2010.2070470.

[26] C. Hu, Modern Semiconductor Devices for Integrated Circuits, Pearson, 2010.

[27] J. A. del Alamo, Nanometre-scale electronics with III-V compound semiconductors, Nature 479 (2011) 317–323. https://doi.org/10.1038/nature10677.

[28] M. Xiao, C. Qiu, Z. Zhang, L. M. Peng, Atomic-layer-deposition growth of an ultrathin HfO_2 film on graphene, ACS Applied Materials & Interfaces 9 (2017) 34050–34056. https://doi.org/10.1021/acsami.7b09408.

[29] S. Anand, A. Singh, S. I. Amin, A. S. Thool, Design and Performance Analysis of Dielectrically Modulated Doping-Less Tunnel FET-Based Label Free Biosensor, IEEE Sensors J. 19 (2019) 4369–4376. https://doi.org/10.1109/JSEN.2019.2900092.

[30] A. Bhattacharyya, M. Chanda, d. De, Performance Assessment of New Dual-Pocket Vertical Heterostructure Tunnel FET-Based Biosensor Considering Steric Hindrance Issue, IEEE Trans. Electron Devices (2019) 1–6. https://doi.org/10.1109/TED.2019.2928850.

LIST OF PUBLICATIONS

1. **Shishir Bhargav** and Sumit Kale, “Design and Simulation of a Pocket-Engineered Dielectric-Modulated TFET Biosensor for Label-Free Breast Cancer Detection,” submitted to *Silicon*, Springer Nature, 2026.

APPENDIX A: SILVACO ATLAS SIMULATION SCRIPT

```
# ========================================================================
# POCKET-ENGINEERED DIELECTRIC-MODULATED TFET BIOSENSOR SIMULATION DECK
# Project Dissertation: Evaluation of Breast Cancer Permittivity Sensitivity
# Target Biomolecules: Air (k=1.0), MCF-10A (k=4.5), Hs578T (k=22.0),
#                      MDA-MB-231 (k=24.5), MCF-7 (k=27.5), T47D (k=32.0)
# ========================================================================

# ------------------------------------------------------------------------
# MODULE 1: INTERFACING BASELINE SIMULATION PROFILE (VACUUM CAVITY CONDITIONS)
# ------------------------------------------------------------------------
go atlas

# Setting fine spatial discretization limits for advanced nonlocal tunneling verification
mesh space.mult=1.0

# Precise X-mesh definition covering the 3nm InAs pocket and nanocavity coordinates
x.mesh loc=-0.002 spacing=0.001
x.mesh loc=0.000  spacing=0.001
x.mesh loc=0.015  spacing=0.001
x.mesh loc=0.020  spacing=0.00005
x.mesh loc=0.023  spacing=0.00005
x.mesh loc=0.031  spacing=0.0001
x.mesh loc=0.042  spacing=0.00005
x.mesh loc=0.062  spacing=0.001
x.mesh loc=0.064  spacing=0.001

# Y-mesh mesh distribution establishing thin spatial inversion layer grid
y.mesh loc=-0.002 spacing=0.001
y.mesh loc=0.000  spacing=0.001
y.mesh loc=0.005  spacing=0.0005
y.mesh loc=0.006  spacing=0.0002
y.mesh loc=0.011  spacing=0.0005
y.mesh loc=0.016  spacing=0.001
y.mesh loc=0.021  spacing=0.0005
y.mesh loc=0.027  spacing=0.001
y.mesh loc=0.029  spacing=0.001

# Sub-surface quantum meshing configuration grid across source-channel interface
qtx.mesh loc=0.015 spac=2.5e-4
qtx.mesh loc=0.020 spac=5.0e-5
```

```
qtx.mesh loc=0.023 spac=5.0e-5
qtx.mesh loc=0.031 spac=1.0e-4
qtx.mesh loc=0.042 spac=5.0e-5
qtx.mesh loc=0.047 spac=2.5e-4

qty.mesh loc=0.006 spac=5.0e-4
qty.mesh loc=0.011 spac=2.0e-4
qty.mesh loc=0.013 spac=2.0e-4
qty.mesh loc=0.014 spac=2.0e-4
qty.mesh loc=0.016 spac=5.0e-4
qty.mesh loc=0.021 spac=5.0e-4

# Structuring device layers: bulk silicon, high-k drain oxide, and low-k source oxide
region num=1 material=Air       x.min=-0.002 x.max=0.064 y.min=-0.002 y.max=0.029
region num=2 material=Silicon   x.min=0.000  x.max=0.062 y.min=0.006  y.max=0.021
region num=11 material=InAs     x.min=0.020  x.max=0.023 y.min=0.006  y.max=0.021
region num=3 material=Silicon   x.min=0.023  x.max=0.031 y.min=0.006  y.max=0.021
region num=10 material=Silicon  x.min=0.031  x.max=0.042 y.min=0.011  y.max=0.016
region num=4 material=HfO2      x.min=0.031  x.max=0.062 y.min=0.000  y.max=0.011
region num=5 material=SiO2      x.min=0.000  x.max=0.031 y.min=0.005  y.max=0.006
region num=6 material=SiO2      x.min=0.000  x.max=0.031 y.min=0.021  y.max=0.022
region num=7 material=HfO2      x.min=0.031  x.max=0.062 y.min=0.016  y.max=0.027

# Defining the dual-nanocavity sensing voids mapping to the geometry
region num=8 user.material=cavity x.min=0.020 x.max=0.031 y.min=0.000 y.max=0.005
region num=9 user.material=cavity x.min=0.020 x.max=0.031 y.min=0.022 y.max=0.027

# Attaching terminal electrode configurations
electrode name=gate  x.min=0.020 x.max=0.042 y.min=-0.001 y.max=0.000
electrode name=gate2 x.min=0.020 x.max=0.042 y.min=0.027  y.max=0.028
electrode name=source x.min=-0.002 x.max=0.000 y.min=0.006 y.max=0.021
electrode name=drain  x.min=0.062  x.max=0.064 y.min=0.011 y.max=0.016

# Mapping the asymmetric doping concentrations matching device architecture
doping uniform p.type conc=1e20 x.min=0.000 x.max=0.020 y.min=0.006 y.max=0.021
doping uniform n.type conc=1e18 x.min=0.042 x.max=0.062 y.min=0.011 y.max=0.016
doping uniform n.type conc=1e12 x.min=0.020 x.max=0.031 y.min=0.006 y.max=0.021
doping uniform n.type conc=1e12 x.min=0.031 x.max=0.042 y.min=0.006 y.max=0.021

# Initializing vacuum baseline conditions inside the variable cavity space
material material=cavity user.group=insulator user.default=oxide permittivity=1.0

# Setting target contact metal work functions
contact name=gate work=4.1
contact name=gate2 work=4.1 common=gate
contact name=source
contact name=drain

# Calibrating transport models: Nonlocal BTBT, Lombardi CVT, SRH, and Fermi Dirac
models srh boltzmann fermi cvt bgn bbt.nonlocal qtunn.dir=xdir

# Setting up custom high-convergence solver convergence criteria
method newton trap maxtraps=50
output p.quantum band.temp con.band val.band band.par
```

```
solve init
solve vdrain=1.0 name=drain
log outf="Air_K1.log"
solve vgate=0.0 name=gate vstep=0.1 vfinal=2.0
log off
save outf="Air_K1.str"

# Mathematical extraction statements logging baseline DC figures of merit
extract init infile="Air_K1.log"
extract name="vt1_Air" (xintercept(maxslope(curve(v."gate",i."drain"))))
extract name="Ion_Air" (max(abs(i."drain")))
extract name="Ioff_Air" (min(abs(i."drain")))
extract name="Ratio_Air" ((max(abs(i."drain")))/(min(abs(i."drain"))))
extract name="gm_Air" (slope(maxslope(curve(abs(v."gate"),abs(i."drain")))))


# -----------------------------------------------------------------------
# MODULE 2: EVALUATION OF HEALTHY MCF-10A RECEPTOR LOADINGS (k = 4.5)
# -----------------------------------------------------------------------
go atlas

mesh space.mult=1.0

x.mesh loc=-0.002 spacing=0.001
x.mesh loc=0.000  spacing=0.001
x.mesh loc=0.015  spacing=0.001
x.mesh loc=0.020  spacing=0.00005
x.mesh loc=0.023  spacing=0.00005
x.mesh loc=0.031  spacing=0.0001
x.mesh loc=0.042  spacing=0.00005
x.mesh loc=0.062  spacing=0.001
x.mesh loc=0.064  spacing=0.001

y.mesh loc=-0.002 spacing=0.001
y.mesh loc=0.000  spacing=0.001
y.mesh loc=0.005  spacing=0.0005
y.mesh loc=0.006  spacing=0.0002
y.mesh loc=0.011  spacing=0.0005
y.mesh loc=0.016  spacing=0.001
y.mesh loc=0.021  spacing=0.0005
y.mesh loc=0.027  spacing=0.001
y.mesh loc=0.029  spacing=0.001

qtx.mesh loc=0.015 spac=2.5e-4
qtx.mesh loc=0.020 spac=5.0e-5
qtx.mesh loc=0.023 spac=5.0e-5
qtx.mesh loc=0.031 spac=1.0e-4
qtx.mesh loc=0.042 spac=5.0e-5
qtx.mesh loc=0.047 spac=2.5e-4

qty.mesh loc=0.006 spac=5.0e-4
qty.mesh loc=0.011 spac=2.0e-4
qty.mesh loc=0.013 spac=2.0e-4
qty.mesh loc=0.014 spac=2.0e-4
qty.mesh loc=0.016 spac=5.0e-4
```

```
qty.mesh loc=0.021 spac=5.0e-4

region num=1 material=Air       x.min=-0.002 x.max=0.064 y.min=-0.002 y.max=0.029
region num=2 material=Silicon   x.min=0.000  x.max=0.062 y.min=0.006  y.max=0.021
region num=11 material=InAs     x.min=0.020  x.max=0.023 y.min=0.006  y.max=0.021
region num=3 material=Silicon   x.min=0.023  x.max=0.031 y.min=0.006  y.max=0.021
region num=10 material=Silicon  x.min=0.031  x.max=0.042 y.min=0.011  y.max=0.016
region num=4 material=HfO2      x.min=0.031  x.max=0.062 y.min=0.000  y.max=0.011
region num=5 material=SiO2      x.min=0.000  x.max=0.031 y.min=0.005  y.max=0.006
region num=6 material=SiO2      x.min=0.000  x.max=0.031 y.min=0.021  y.max=0.022
region num=7 material=HfO2      x.min=0.031  x.max=0.062 y.min=0.016  y.max=0.027

region num=8 user.material=cavity x.min=0.020 x.max=0.031 y.min=0.000 y.max=0.005
region num=9 user.material=cavity x.min=0.020 x.max=0.031 y.min=0.022 y.max=0.027

electrode name=gate  x.min=0.020 x.max=0.042 y.min=-0.001 y.max=0.000
electrode name=gate2 x.min=0.020 x.max=0.042 y.min=0.027  y.max=0.028
electrode name=source x.min=-0.002 x.max=0.000 y.min=0.006 y.max=0.021
electrode name=drain  x.min=0.062  x.max=0.064 y.min=0.011 y.max=0.016

doping uniform p.type conc=1e20 x.min=0.000 x.max=0.020 y.min=0.006 y.max=0.021
doping uniform n.type conc=1e18 x.min=0.042 x.max=0.062 y.min=0.011 y.max=0.016
doping uniform n.type conc=1e12 x.min=0.020 x.max=0.031 y.min=0.006 y.max=0.021
doping uniform n.type conc=1e12 x.min=0.031 x.max=0.042 y.min=0.006 y.max=0.021

# Adjusting permittivity factor mapping to standard MCF-10A biological structures
material material=cavity user.group=insulator user.default=oxide permittivity=4.5

contact name=gate work=4.1
contact name=gate2 work=4.1 common=gate
contact name=source
contact name=drain

models srh boltzmann fermi cvt bgn bbt.nonlocal qtunn.dir=xdir

method newton trap maxtraps=50
output p.quantum band.temp con.band val.band band.par

solve init
solve vdrain=1.0 name=drain
log outf="MCF10A_K4.5.log"
solve vgate=0.0 name=gate vstep=0.1 vfinal=2.0
log off
save outf="MCF10A_K4.5.str"

extract init infile="MCF10A_K4.5.log"
extract name="vt1_MCF10A" (xintercept(maxslope(curve(v."gate",i."drain"))))
extract name="Ion_MCF10A" (max(abs(i."drain")))
extract name="Ioff_MCF10A" (min(abs(i."drain")))
extract name="Ratio_MCF10A" ((max(abs(i."drain")))/(min(abs(i."drain"))))
extract name="gm_MCF10A" (slope(maxslope(curve(abs(v."gate"),abs(i."drain")))))


# ------------------------------------------------------------------------
# MODULE 3: CHARACTERIZING MALIGNANT Hs578T VARIANT IMMOBILIZATION (k = 22.0)
```

```
# ----------------------------------------------------------------------
go atlas

mesh space.mult=1.0

x.mesh loc=-0.002 spacing=0.001
x.mesh loc=0.000  spacing=0.001
x.mesh loc=0.015  spacing=0.001
x.mesh loc=0.020  spacing=0.00005
x.mesh loc=0.023  spacing=0.00005
x.mesh loc=0.031  spacing=0.0001
x.mesh loc=0.042  spacing=0.00005
x.mesh loc=0.062  spacing=0.001
x.mesh loc=0.064  spacing=0.001

y.mesh loc=-0.002 spacing=0.001
y.mesh loc=0.000  spacing=0.001
y.mesh loc=0.005  spacing=0.0005
y.mesh loc=0.006  spacing=0.0002
y.mesh loc=0.011  spacing=0.0005
y.mesh loc=0.016  spacing=0.001
y.mesh loc=0.021  spacing=0.0005
y.mesh loc=0.027  spacing=0.001
y.mesh loc=0.029  spacing=0.001

qtx.mesh loc=0.015 spac=2.5e-4
qtx.mesh loc=0.020 spac=5.0e-5
qtx.mesh loc=0.023 spac=5.0e-5
qtx.mesh loc=0.031 spac=1.0e-4
qtx.mesh loc=0.042 spac=5.0e-5
qtx.mesh loc=0.047 spac=2.5e-4

qty.mesh loc=0.006 spac=5.0e-4
qty.mesh loc=0.011 spac=2.0e-4
qty.mesh loc=0.013 spac=2.0e-4
qty.mesh loc=0.014 spac=2.0e-4
qty.mesh loc=0.016 spac=5.0e-4
qty.mesh loc=0.021 spac=5.0e-4

region num=1 material=Air       x.min=-0.002 x.max=0.064 y.min=-0.002 y.max=0.029
region num=2 material=Silicon   x.min=0.000  x.max=0.062 y.min=0.006  y.max=0.021
region num=11 material=InAs     x.min=0.020  x.max=0.023 y.min=0.006  y.max=0.021
region num=3 material=Silicon   x.min=0.023  x.max=0.031 y.min=0.006  y.max=0.021
region num=10 material=Silicon  x.min=0.031  x.max=0.042 y.min=0.011  y.max=0.016
region num=4 material=HfO2      x.min=0.031  x.max=0.062 y.min=0.000  y.max=0.011
region num=5 material=SiO2      x.min=0.000  x.max=0.031 y.min=0.005  y.max=0.006
region num=6 material=SiO2      x.min=0.000  x.max=0.031 y.min=0.021  y.max=0.022
region num=7 material=HfO2      x.min=0.031  x.max=0.062 y.min=0.016  y.max=0.027

region num=8 user.material=cavity x.min=0.020 x.max=0.031 y.min=0.000 y.max=0.005
region num=9 user.material=cavity x.min=0.020 x.max=0.031 y.min=0.022 y.max=0.027

electrode name=gate  x.min=0.020 x.max=0.042 y.min=-0.001 y.max=0.000
electrode name=gate2 x.min=0.020 x.max=0.042 y.min=0.027  y.max=0.028
electrode name=source x.min=-0.002 x.max=0.000 y.min=0.006 y.max=0.021
```

```
electrode name=drain  x.min=0.062  x.max=0.064 y.min=0.011 y.max=0.016

doping uniform p.type conc=1e20 x.min=0.000 x.max=0.020 y.min=0.006 y.max=0.021
doping uniform n.type conc=1e18 x.min=0.042 x.max=0.062 y.min=0.011 y.max=0.016
doping uniform n.type conc=1e12 x.min=0.020 x.max=0.031 y.min=0.006 y.max=0.021
doping uniform n.type conc=1e12 x.min=0.031 x.max=0.042 y.min=0.006 y.max=0.021

# Mapping localized electrostatic field changes generated by Hs578T cells
material material=cavity user.group=insulator user.default=oxide permittivity=22.0

contact name=gate work=4.1
contact name=gate2 work=4.1 common=gate
contact name=source
contact name=drain

models srh boltzmann fermi cvt bgn bbt.nonlocal qtunn.dir=xdir

method newton trap maxtraps=50
output p.quantum band.temp con.band val.band band.par

solve init
solve vdrain=1.0 name=drain
log outf="Hs578T_K22.log"
solve vgate=0.0 name=gate vstep=0.1 vfinal=2.0
log off
save outf="Hs578T_K22.str"

extract init infile="Hs578T_K22.log"
extract name="vt1_Hs578T" (xintercept(maxslope(curve(v."gate",i."drain"))))
extract name="Ion_Hs578T" (max(abs(i."drain")))
extract name="Ioff_Hs578T" (min(abs(i."drain")))
extract name="Ratio_Hs578T" ((max(abs(i."drain")))/(min(abs(i."drain"))))
extract name="gm_Hs578T" (slope(maxslope(curve(abs(v."gate"),abs(i."drain")))))


# ------------------------------------------------------------------------
# MODULE 4: TRACKING MALIGNANT MDA-MB-231 TARGET PHENOTYPES (k = 24.5)
# ------------------------------------------------------------------------
go atlas

mesh space.mult=1.0

x.mesh loc=-0.002 spacing=0.001
x.mesh loc=0.000  spacing=0.001
x.mesh loc=0.015  spacing=0.001
x.mesh loc=0.020  spacing=0.00005
x.mesh loc=0.023  spacing=0.00005
x.mesh loc=0.031  spacing=0.0001
x.mesh loc=0.042  spacing=0.00005
x.mesh loc=0.062  spacing=0.001
x.mesh loc=0.064  spacing=0.001

y.mesh loc=-0.002 spacing=0.001
y.mesh loc=0.000  spacing=0.001
y.mesh loc=0.005  spacing=0.0005
```

```
y.mesh loc=0.006  spacing=0.0002
y.mesh loc=0.011  spacing=0.0005
y.mesh loc=0.016  spacing=0.001
y.mesh loc=0.021  spacing=0.0005
y.mesh loc=0.027  spacing=0.001
y.mesh loc=0.029  spacing=0.001

qtx.mesh loc=0.015 spac=2.5e-4
qtx.mesh loc=0.020 spac=5.0e-5
qtx.mesh loc=0.023 spac=5.0e-5
qtx.mesh loc=0.031 spac=1.0e-4
qtx.mesh loc=0.042 spac=5.0e-5
qtx.mesh loc=0.047 spac=2.5e-4

qty.mesh loc=0.006 spac=5.0e-4
qty.mesh loc=0.011 spac=2.0e-4
qty.mesh loc=0.013 spac=2.0e-4
qty.mesh loc=0.014 spac=2.0e-4
qty.mesh loc=0.016 spac=5.0e-4
qty.mesh loc=0.021 spac=5.0e-4

region num=1 material=Air       x.min=-0.002 x.max=0.064 y.min=-0.002 y.max=0.029
region num=2 material=Silicon   x.min=0.000  x.max=0.062 y.min=0.006  y.max=0.021
region num=11 material=InAs     x.min=0.020  x.max=0.023 y.min=0.006  y.max=0.021
region num=3 material=Silicon   x.min=0.023  x.max=0.031 y.min=0.006  y.max=0.021
region num=10 material=Silicon  x.min=0.031  x.max=0.042 y.min=0.011  y.max=0.016
region num=4 material=HfO2      x.min=0.031  x.max=0.062 y.min=0.000  y.max=0.011
region num=5 material=SiO2      x.min=0.000  x.max=0.031 y.min=0.005  y.max=0.006
region num=6 material=SiO2      x.min=0.000  x.max=0.031 y.min=0.021  y.max=0.022
region num=7 material=HfO2      x.min=0.031  x.max=0.062 y.min=0.016  y.max=0.027

region num=8 user.material=cavity x.min=0.020 x.max=0.031 y.min=0.000 y.max=0.005
region num=9 user.material=cavity x.min=0.020 x.max=0.031 y.min=0.022 y.max=0.027

electrode name=gate  x.min=0.020 x.max=0.042 y.min=-0.001 y.max=0.000
electrode name=gate2 x.min=0.020 x.max=0.042 y.min=0.027  y.max=0.028
electrode name=source x.min=-0.002 x.max=0.000 y.min=0.006 y.max=0.021
electrode name=drain  x.min=0.062  x.max=0.064 y.min=0.011 y.max=0.016

doping uniform p.type conc=1e20 x.min=0.000 x.max=0.020 y.min=0.006 y.max=0.021
doping uniform n.type conc=1e18 x.min=0.042 x.max=0.062 y.min=0.011 y.max=0.016
doping uniform n.type conc=1e12 x.min=0.020 x.max=0.031 y.min=0.006 y.max=0.021
doping uniform n.type conc=1e12 x.min=0.031 x.max=0.042 y.min=0.006 y.max=0.021

# Assembling correct calibrated relative permittivity assignments based on clinical guidelin
material material=cavity user.group=insulator user.default=oxide permittivity=24.5

contact name=gate work=4.1
contact name=gate2 work=4.1 common=gate
contact name=source
contact name=drain

models srh boltzmann fermi cvt bgn bbt.nonlocal qtunn.dir=xdir

method newton trap maxtraps=50
```

```
output p.quantum band.temp con.band val.band band.par

solve init
solve vdrain=1.0 name=drain
log outf="MDA_K24.5.log"
solve vgate=0.0 name=gate vstep=0.1 vfinal=2.0
log off
save outf="MDA_K24.5.str"

extract init infile="MDA_K24.5.log"
extract name="vt1_MDA" (xintercept(maxslope(curve(v."gate",i."drain"))))
extract name="Ion_MDA" (max(abs(i."drain")))
extract name="Ioff_MDA" (min(abs(i."drain")))
extract name="Ratio_MDA" ((max(abs(i."drain")))/(min(abs(i."drain"))))
extract name="gm_MDA" (slope(maxslope(curve(abs(v."gate"),abs(i."drain")))))


# ----------------------------------------------------------------------
# MODULE 5: PROFILE RUN OVER MALIGNANT MCF-7 STRAINS (k = 27.5)
# ----------------------------------------------------------------------
go atlas

mesh space.mult=1.0

x.mesh loc=-0.002 spacing=0.001
x.mesh loc=0.000  spacing=0.001
x.mesh loc=0.015  spacing=0.001
x.mesh loc=0.020  spacing=0.00005
x.mesh loc=0.023  spacing=0.00005
x.mesh loc=0.031  spacing=0.0001
x.mesh loc=0.042  spacing=0.00005
x.mesh loc=0.062  spacing=0.001
x.mesh loc=0.064  spacing=0.001

y.mesh loc=-0.002 spacing=0.001
y.mesh loc=0.000  spacing=0.001
y.mesh loc=0.005  spacing=0.0005
y.mesh loc=0.006  spacing=0.0002
y.mesh loc=0.011  spacing=0.0005
y.mesh loc=0.016  spacing=0.001
y.mesh loc=0.021  spacing=0.0005
y.mesh loc=0.027  spacing=0.001
y.mesh loc=0.029  spacing=0.001

qtx.mesh loc=0.015 spac=2.5e-4
qtx.mesh loc=0.020 spac=5.0e-5
qtx.mesh loc=0.023 spac=5.0e-5
qtx.mesh loc=0.031 spac=1.0e-4
qtx.mesh loc=0.042 spac=5.0e-5
qtx.mesh loc=0.047 spac=2.5e-4

qty.mesh loc=0.006 spac=5.0e-4
qty.mesh loc=0.011 spac=2.0e-4
qty.mesh loc=0.013 spac=2.0e-4
qty.mesh loc=0.014 spac=2.0e-4
```

```
qty.mesh loc=0.016 spac=5.0e-4
qty.mesh loc=0.021 spac=5.0e-4

region num=1 material=Air       x.min=-0.002 x.max=0.064 y.min=-0.002 y.max=0.029
region num=2 material=Silicon   x.min=0.000  x.max=0.062 y.min=0.006  y.max=0.021
region num=11 material=InAs     x.min=0.020  x.max=0.023 y.min=0.006  y.max=0.021
region num=3 material=Silicon   x.min=0.023  x.max=0.031 y.min=0.006  y.max=0.021
region num=10 material=Silicon  x.min=0.031  x.max=0.042 y.min=0.011  y.max=0.016
region num=4 material=HfO2      x.min=0.031  x.max=0.062 y.min=0.000  y.max=0.011
region num=5 material=SiO2      x.min=0.000  x.max=0.031 y.min=0.005  y.max=0.006
region num=6 material=SiO2      x.min=0.000  x.max=0.031 y.min=0.021  y.max=0.022
region num=7 material=HfO2      x.min=0.031  x.max=0.062 y.min=0.016  y.max=0.027

region num=8 user.material=cavity x.min=0.020 x.max=0.031 y.min=0.000 y.max=0.005
region num=9 user.material=cavity x.min=0.020 x.max=0.031 y.min=0.022 y.max=0.027

electrode name=gate  x.min=0.020 x.max=0.042 y.min=-0.001 y.max=0.000
electrode name=gate2 x.min=0.020 x.max=0.042 y.min=0.027  y.max=0.028
electrode name=source x.min=-0.002 x.max=0.000 y.min=0.006 y.max=0.021
electrode name=drain  x.min=0.062  x.max=0.064 y.min=0.011 y.max=0.016

doping uniform p.type conc=1e20 x.min=0.000 x.max=0.020 y.min=0.006 y.max=0.021
doping uniform n.type conc=1e18 x.min=0.042 x.max=0.062 y.min=0.011 y.max=0.016
doping uniform n.type conc=1e12 x.min=0.020 x.max=0.031 y.min=0.006 y.max=0.021
doping uniform n.type conc=1e12 x.min=0.031 x.max=0.042 y.min=0.006 y.max=0.021

# Mapping increased dielectric modulation factor representing complete MCF-7 cell filling
material material=cavity user.group=insulator user.default=oxide permittivity=27.5

contact name=gate work=4.1
contact name=gate2 work=4.1 common=gate
contact name=source
contact name=drain

models srh boltzmann fermi cvt bgn bbt.nonlocal qtunn.dir=xdir

method newton trap maxtraps=50
output p.quantum band.temp con.band val.band band.par

solve init
solve vdrain=1.0 name=drain
log outf="MCF7_K27.5.log"
solve vgate=0.0 name=gate vstep=0.1 vfinal=2.0
log off
save outf="MCF7_K27.5.str"

extract init infile="MCF7_K27.5.log"
extract name="vt1_MCF7" (xintercept(maxslope(curve(v."gate",i."drain"))))
extract name="Ion_MCF7" (max(abs(i."drain")))
extract name="Ioff_MCF7" (min(abs(i."drain")))
extract name="Ratio_MCF7" ((max(abs(i."drain")))/(min(abs(i."drain"))))
extract name="gm_MCF7" (slope(maxslope(curve(abs(v."gate"),abs(i."drain")))))


# ------------------------------------------------------------------------
```

```
# MODULE 6: SIMULATION ITERATION FOR HIGH-RISK T47D TUMOR VARIANT (k = 32.0)
# -----------------------------------------------------------------------
go atlas

mesh space.mult=1.0

x.mesh loc=-0.002 spacing=0.001
x.mesh loc=0.000  spacing=0.001
x.mesh loc=0.015  spacing=0.001
x.mesh loc=0.020  spacing=0.00005
x.mesh loc=0.023  spacing=0.00005
x.mesh loc=0.031  spacing=0.0001
x.mesh loc=0.042  spacing=0.00005
x.mesh loc=0.062  spacing=0.001
x.mesh loc=0.064  spacing=0.001

y.mesh loc=-0.002 spacing=0.001
y.mesh loc=0.000  spacing=0.001
y.mesh loc=0.005  spacing=0.0005
y.mesh loc=0.006  spacing=0.0002
y.mesh loc=0.011  spacing=0.0005
y.mesh loc=0.016  spacing=0.001
y.mesh loc=0.021  spacing=0.0005
y.mesh loc=0.027  spacing=0.001
y.mesh loc=0.029  spacing=0.001

qtx.mesh loc=0.015 spac=2.5e-4
qtx.mesh loc=0.020 spac=5.0e-5
qtx.mesh loc=0.023 spac=5.0e-5
qtx.mesh loc=0.031 spac=1.0e-4
qtx.mesh loc=0.042 spac=5.0e-5
qtx.mesh loc=0.047 spac=2.5e-4

qty.mesh loc=0.006 spac=5.0e-4
qty.mesh loc=0.011 spac=2.0e-4
qty.mesh loc=0.013 spac=2.0e-4
qty.mesh loc=0.014 spac=2.0e-4
qty.mesh loc=0.016 spac=5.0e-4
qty.mesh loc=0.021 spac=5.0e-4

region num=1 material=Air       x.min=-0.002 x.max=0.064 y.min=-0.002 y.max=0.029
region num=2 material=Silicon   x.min=0.000  x.max=0.062 y.min=0.006  y.max=0.021
region num=11 material=InAs     x.min=0.020  x.max=0.023 y.min=0.006  y.max=0.021
region num=3 material=Silicon   x.min=0.023  x.max=0.031 y.min=0.006  y.max=0.021
region num=10 material=Silicon  x.min=0.031  x.max=0.042 y.min=0.011  y.max=0.016
region num=4 material=HfO2      x.min=0.031  x.max=0.062 y.min=0.000  y.max=0.011
region num=5 material=SiO2      x.min=0.000  x.max=0.031 y.min=0.005  y.max=0.006
region num=6 material=SiO2      x.min=0.000  x.max=0.031 y.min=0.021  y.max=0.022
region num=7 material=HfO2      x.min=0.031  x.max=0.062 y.min=0.016  y.max=0.027

region num=8 user.material=cavity x.min=0.020 x.max=0.031 y.min=0.000 y.max=0.005
region num=9 user.material=cavity x.min=0.020 x.max=0.031 y.min=0.022 y.max=0.027

electrode name=gate  x.min=0.020 x.max=0.042 y.min=-0.001 y.max=0.000
electrode name=gate2 x.min=0.020 x.max=0.042 y.min=0.027  y.max=0.028
```

```
electrode name=source x.min=-0.002 x.max=0.000 y.min=0.006 y.max=0.021
electrode name=drain  x.min=0.062  x.max=0.064 y.min=0.011 y.max=0.016

doping uniform p.type conc=1e20 x.min=0.000 x.max=0.020 y.min=0.006 y.max=0.021
doping uniform n.type conc=1e18 x.min=0.042 x.max=0.062 y.min=0.011 y.max=0.016
doping uniform n.type conc=1e12 x.min=0.020 x.max=0.031 y.min=0.006 y.max=0.021
doping uniform n.type conc=1e12 x.min=0.031 x.max=0.042 y.min=0.006 y.max=0.021

# Calibrating the peak permittivity constant (k=32) tracking maximum band bending
material material=cavity user.group=insulator user.default=oxide permittivity=32.0

contact name=gate work=4.1
contact name=gate2 work=4.1 common=gate
contact name=source
contact name=drain

models srh boltzmann fermi cvt bgn bbt.nonlocal qtunn.dir=xdir

method newton trap maxtraps=50
output p.quantum band.temp con.band val.band band.par

solve init
solve vdrain=1.0 name=drain
log outf="T47D_K32.log"
solve vgate=0.0 name=gate vstep=0.1 vfinal=2.0
log off
save outf="T47D_K32.str"

# Final parameters log execution matching maximum threshold shift constraints
extract init infile="T47D_K32.log"
extract name="vt1_T47D" (xintercept(maxslope(curve(v."gate",i."drain"))))
extract name="Ion_T47D" (max(abs(i."drain")))
extract name="Ioff_T47D" (min(abs(i."drain")))
extract name="Ratio_T47D" ((max(abs(i."drain")))/(min(abs(i."drain"))))
extract name="gm_T47D" (slope(maxslope(curve(abs(v."gate"),abs(i."drain")))))

quit
```

Shishir Report

ORIGINALITY REPORT

9%	3%	8%	1%
SIMILARITY INDEX	INTERNET SOURCES	PUBLICATIONS	STUDENT PAPERS

PRIMARY SOURCES

#	Source	%
1	nvhrbiblio.nl Internet Source	1%
2	Simon Deleonibus. "Emerging Devices for Low-Power and High-Performance Nanosystems - Physics, Novel Functions, and Data Processing", CRC Press, 2018 Publication	1%
3	Jagadesh Kumar Mamidala, Rajat Vishnoi, Pratyush Pandey. "Tunnel Field-Effect Transistors (TFET)", Wiley, 2016 Publication	1%
4	Sukanya Ghosh. "Performance evaluation of charge plasma based dielectrically tuned JFTFET for label-free detection of breast cancer biomarkers", Micro and Nanostructures, 2025 Publication	1%
5	M. Pavan Kumar, Srinivasa Rao Karumuri, Ch. V. Ravi Sankar, K. L. V. Ramana Kumari et al. "Performance assessment of dielectrically	1%

modulated dual metal gate Ge/Si heterostructure TFET for detection of biomolecules: as a biosensor", Microsystem Technologies, 2025
Publication

6	Ranjith Kumar T, Lakshmi Priya G. "Ultra-sensitive dengue NS1 protein detection via asymmetric source-drain, heterojunction and dual-dielectric cavities in a uniform tunnel FET biosensor", Results in Engineering, 2024 Publication	1%
7	Tunneling Field Effect Transistor Technology, 2016. Publication	1%
8	Simon Deleonibus. "Intelligent Integrated Systems - Devices, Technologies, and Architectures", Pan Stanford, 2019 Publication	<1%
9	Chandan Kumar Sarkar. "Technology Computer Aided Design - Simulation for VLSI MOSFET", CRC Press, 2019 Publication	<1%
10	Krzysztof Iniewski, Santosh K. Kurinec, Sumeet Walia. "Energy Efficient Computing & Electronics - Devices to Systems", CRC Press, 2019 Publication	<1%

11	ethesis.nitrkl.ac.in Internet Source	<1%
12	Khurshed Ahmad Shah. "Nanoelectronics - Advanced Concepts and Device Applications", Routledge, 2025 Publication	<1%
13	Sneha. M. Joseph, Nameirakpam Premjit Singh, K. Vanlalawmpuia. "High Performance Dielectrically Modulated Germanium Source Extended Double Gate Tunnel Field Effect Transistor for Biosensing Applications", Springer Science and Business Media LLC, 2025 Publication	<1%
14	repository.iiitd.edu.in Internet Source	<1%
15	Priyanka Karmakar, Prasanna Kumar Sahu. "Performance assessment of a modified gate oxide TFET as a biosensor for breast cancer cell detection", Microsystem Technologies, 2025 Publication	<1%
16	James E. Morris, Krzysztof Iniewski. "Nanoelectronic Device Applications Handbook", CRC Press, 2017 Publication	<1%

17	Johnson, Micha. "Advancements in the Solid-state Impact-ionization Multiplier (SIM) Through Simulation, Fabrication, and Characterization", Proquest, 2012. Publication	<1 %
18	Naveen Kumar, Prateek Kumar, Ankit Dixit, Prabhat Singh. "Classical to Quantum Transport in Multi-Dimensional Field Effect Transistors", CRC Press, 2025 Publication	<1 %
19	Qing Zhang. "Carbon Nanotubes and Their Applications", Pan Stanford, 2019 Publication	<1 %
20	Christian Piguet. "Low-Power CMOS Circuits - Technology, Logic Design and CAD Tools", CRC Press, 2018 Publication	<1 %
21	Ramesh, An. "Tunneling based quantum functional devices and circuits for low power VLSI design", Proquest, 2014. Publication	<1 %
22	Hindupur, Ramya. "Modeling floating body memory devices", Proquest, 20111108 Publication	<1 %
23	Vasireddy, Vivek. "Experimental and simulation results of a 0.15mum FlexFET transistor", Proquest, 20111108	<1 %

Publication

24	Dragica Vasileska, Stephen M. Goodnick, Gerhard Klimeck. "Computational Electronics - Semiclassical and Quantum Device Modeling and Simulation", CRC Press, 2017 Publication	<1%
25	Lee, Hyun Jung. "Top-gate nanocrystalline silicon thin film transistors", Proquest, 20111109 Publication	<1%

Exclude quotes	On	Exclude matches	Off
Exclude bibliography	On		